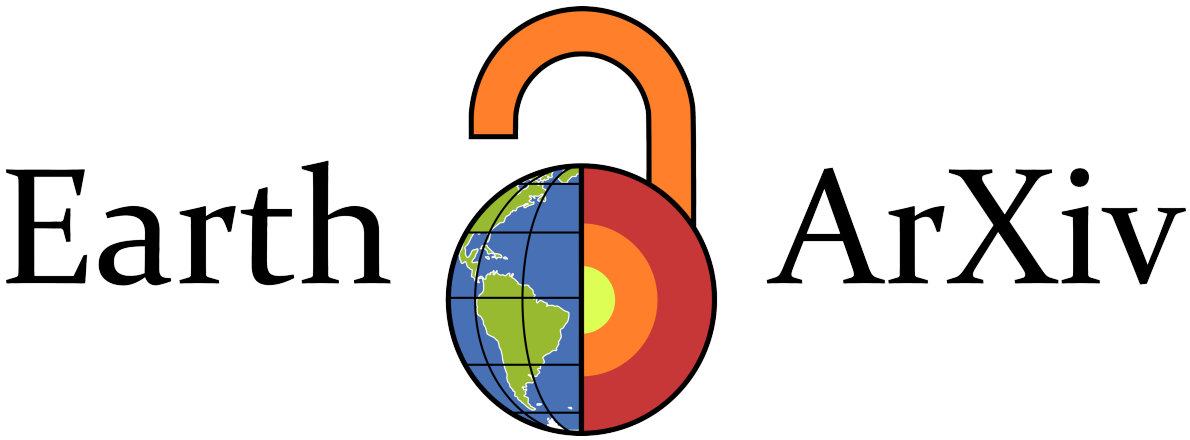

Agent-based Modelling of Microbialite Formation through Sedimentation and Precipitation Dynamics

Niall Rodgers* [1,2], Laurane Fogret [3], Mark van Zuilen [3], H. James Cleaves [4,5,6], Sudha Rajamani [7], and Sean McMahon [1,2,8]

[1]*UK Centre for Astrobiology, School of Physics and Astronomy, University of Edinburgh, United Kingdom*
[2]*Edinburgh Centre for Planetary Sciences, University of Edinburgh, United Kingdom*
[3]*Naturalis Biodiversity Center, Leiden, 2333CR, The Netherlands*
[4]*Department of Chemistry, Howard University, Washington, DC 20059, USA*
[5]*Earth and Planets Laboratory, Carnegie Institution for Science Washington , DC 20015, USA*
[6]*Blue Marble Space Institute for Science, Seattle, WA 98104, USA*
[7]*Department of Biology, IISER Pune, Pune, Maharashtra, India*
[8]*School of Geosciences, University of Edinburgh, United Kingdom*

April 10, 2026

Abstract

Fossil microbialites resulting from the interplay of sedimentation and microbially induced precipitation are among the oldest evidence of life on Earth and help geobiologists interpret many sedimentary environments. However, the factors governing their internal structure and external morphology are still poorly understood. Additionally, abiotic processes can mimic the morphology of some microbialites, complicating their use as "biosignatures". The presence and style of internal structures such as clots and laminations may help solve both problems, but existing models of microbialite growth address only external morphology and do not show explicitly how internal structures emerge. In this work, we present an agent-based model of microbialite formation using a fast, open-source, high-level microbialite modelling framework, written in Julia. We separate and label sedimentation and microbially induced precipitation, and allow external periodic forcing to control either or both. We qualitatively reproduce a wide range of internal and external morphologies found in real microbialites. Importantly, we find that microbialites with the same external morphology can differ greatly in their internal structure, a result that was impossible to observe with previous approaches. Further exploration and extension of our model may offer new approaches to resolving the ambiguity of potential microbialites in the rock record. Finally, we present the first interactive microbialite simulation, that enables live parameter updating through an accessible interface that can be used as a tool for both research and teaching.

*Corresponding author: niall.rodgers@ed.ac.uk

1 Introduction

Microbialites are organosedimentary structures resulting from interactions between microbial communities and their environment, including sedimentary dynamics and mineral precipitation processes [1, 2]. They encompass a wide spectrum of morphologies, from planar to domical or columnar, and internal architectures, commonly classified into stromatolites (laminated), dendrolites (shrublike), thrombolites (clotted) and leiolites (aphanitic or fine-grained) [3].

Understanding microbialites is vital for reconstructing Earth's history, as they provide some of the oldest and most abundant evidence for early life on our planet [4, 5]. These structures can form in a wide variety of environments, including shallow marine, lacustrine, and hydrothermal settings, and are found throughout almost all geological time, from billions of years ago to the present day [6]. Their formation reflects a complex interplay of intrinsic biotic factors and extrinsic environmental controls at the time of deposition [7]. They may also be subject to geological alteration, such as diagenesis and metamorphism. Hence, interpretation of the final microbialite morphology and internal fabric is often difficult, and assessing the biogenicity of some candidate fossils remains a significant challenge [8, 9]. This ambiguity complicates our understanding of the evolution of the Earth's biosphere (as shown by the recent controversy over 3.7 billion year old purported stromatolites in Greenland [10]) and has implications for the search for life beyond Earth [11].

One way to tackle the ambiguity of morphology is to gain a better understanding of the generative processes leading to given structures and thus to assess the role of biology in their formation. Many approaches to this in the literature have focused on qualitative and conceptual models [12, 7]; however, computational models offer an alternative framework to explore microbialite growth in a way that allows hypotheses about the emergence of particular structures to be tested.

Despite this potential, work in this area has been sporadic and real application limited. Continuum models have been proposed that are too general to capture details of the formation process, are not widely used in the microbialite community, and can even lead to contradictory conclusions regarding biogenicity [13, 14, 15, 16]. By contrast, agent-based models can provide more localised insights into the interacting processes that lead to the formation of microbialites. The seminal work by Dupraz, Pattisina, and Verrecchia [17] introduced an agent-based model to simulate microbialite growth, which has been widely cited by the community and recognised for its potential. However, it has not been widely applied, and relies on two decades old `C++` code currently available only on request. In relation to stromatolites, both approaches suffer the same fundamental limitation, which is that visible laminations do not arise from interactions within the models. Although illustrations of these models often appear to show lamination, these are drawn artificially and represent former positions of the external surface during growth. The absence of true internal structure limits the applicability of these models to the whole spectrum of microbialites. The same point was raised by Dupraz, Pattisina, and Verrecchia [17] themselves: "the model does not produce a mechanistic description of the laminae but rather a holistic approach to morphology generation." but has thus far remained unaddressed.

To address this gap, we present a fast high-level agent-based model of microbialite formation, developed in `Julia` using the `Agents.jl` framework. Our model builds upon the approach of Dupraz, Pattisina, and Verrecchia [17] but introduces key enhancements: (i) it explicitly simulates sedimentation and microbially induced precipitation as separate processes, (ii) it allows external periodic forcing to influence layer formation, (iii) it is available publicly and written in a high-level extensible framework, and (iv) it can be run interactively allowing live parameter updates. The model simulates these processes using a framework inspired by diffusion-limited aggregation

(DLA), allowing both mechanisms to be individually labelled and tracked. This demonstrates how macroscopic morphologies and internal fabrics can emerge from the interactions, and stand-alone behaviour, of precipitation and sedimentation.

Firstly, we show how this model can reproduce a wide range of diverse microbialite varieties. We then qualitatively explore the morphospace generated by this model and show how the interactive interface can be used to easily approximate structures subject to sudden morphological changes. Finally, we demonstrate how this model allows the decoupling of internal structure and external morphology highlighting the complexities of microbialite formation. In the supplementary information, we highlight how the model can modified to heuristically generate conical-like objects, subject to limitations, and how various quantitative measurements can be used to understand the model output. Although this high-level model represents an exploratory framework of microbialite formation, it provides a flexible and extensible foundation for future microbialite modelling. Our model directly demonstrates the ambiguity of morphology as a biosignature, since by using simple abstract rules and external periodicity a wide spectrum of morphologies can be generated without any reference to the underlying details of the true mechanisms and its biogenicity.

2 Previous Approaches to Microbialite Modelling

There is a long history of the computational study of microbialites (primarily focused on stromatolites) with simple computer programs implemented by Hofmann [18] over 50 years ago. However, the work has been sporadic and no standard approach has emerged [19]. The state of the numerical modelling described in the decade-old review of Bosak, Knoll, and Petroff [19] remains essentially unchanged. Broadly, two main modelling approaches have been pursued. The first involves representing stromatolite growth through partial differential equations, capturing surface evolution [20, 13, 16, 21, 22]. The second focuses on stochastic agent-based (or process based) models, which aim to simulate the localised, dynamic interactions between sedimentation and microbial processes [17, 23, 24].

2.1 Continuum Models

The continuum modelling of microbialites began with the work of Grotzinger and Rothman [20] who proposed that stromatolites could be modelled by the Kardar–Parisi–Zhang (KPZ) equation, a framework originally developed to describe generic surface growth, where they directly aimed to answer questions of biogenicity. This marked a shift toward viewing stromatolite morphogenesis as a physical process rather than just a biological one. Further work extended and analysed the applicability of KPZ to stromatolites and biogenicity [13, 14, 15, 16, 22].

Despite their foundational role in showing the ambiguity of morphology as an indicator of biogenicity [20], KPZ-based models have significant limitations when used to model microbialites, discussed in detail in Cuerno et al. [16]. Some types of stromatolite morphologies, in particular overhangs, cannot be generated by KPZ models. As a highly general description of interface growth, the KPZ equation offers a limited capacity to distinguish between biotic and abiotic processes, and its terms cannot be directly tied to specific mechanisms of microbialite formation. Additional caveats regarding asymptotic limits are given in Cuerno et al. [16].

An under-emphasised point is that when using KPZ models the layers must be drawn artificially; each layer represents the height of the structure at a particular time, rather than sedimentary or compositional variation of the kind found in real stromatolites in the rock record. The models

also only allow an understanding of gross external morphology and cannot be used for exploring transitions between different microbialite types. Additionally, these are not well suited to the microbialite community as it is difficult for non-mathematical specialists to interpret these equations. Furthermore, it is difficult to test specific hypotheses surrounding biogenicity or formation, although this can be attempted as in Ojakangas, Awramik, and Storrie-Lombardi [22]. For the above reasons, since the initial peak of the 1990s and early 2000s we have seen limited use and uptake of this approach of modelling stromatolites.

One promising approach has been the work of Petroff et al. [21], a physics-based approach, that argues that the shape of conical stromatolites derives from the physics of diffusion through a thin film. This principled approach is promising, however, it is limited to explaining the external morphology of conical stromatolites, modelling the shape of the laminae but not explaining why the layer transition happens. In addition, it behaves in similar ways to the models of the formation of abiotic conical structures, like stalactites and icicles. Abiotic objects of this specific class can be well represented by continuum models, such as those developed by [25], yet this cannot be easily achieved for generic microbialites, due to the complexity of interacting processes and the diversity of objects observed in the fossil record.

Continuum models are an efficient, although potentially mathematically complex, way to capture broad morphological trends, but they often struggle to represent internal structure. In many cases, they are too broad to test real-world hypotheses or draw strong conclusions about biogenicity.

2.2 Agent-based approach

Another approach to model the formation of stromatolites is to use an agent-based model (ABM), where large numbers of agents interacting according to local rules combine to generate emergent morphologies. Exemplified by the seminal work of Dupraz, Pattisina, and Verrecchia [17] where a diffusion-limited aggregation (DLA) model combined with a cellular automata model reproduced a range of microbialitic morphologies. While this model has been widely cited, its direct use or extension in the literature has been limited. The original model reproduces the external morphology, but stromatolitic lamination arises from growth history alone. As far as we are aware, no peer-reviewed article has yet proposed a formal extension of the model. Additionally, this model follows the reproducibly standards of when it was published nearly two decades ago: it is written in `C++` and the source code is only available on request.

Agent-based models (ABMs) have great potential benefit to the study of microbialites, whose morphologies emerge from local interactions. A variety of biological and environmental processes could be represented by interpretable local rules, enabling targeted hypothesis testing and access to internal structural dynamics. A version of this was attempted by Johnson and Grotzinger [23] in 2006 using a process-based numerical model, which attempted to relate sediment type to structural features; however, as the authors state "The model cannot explain detailed morphologic attributes", leading to this work being underappreciated by the community. Metazoan–microbial reef growth was simulated in the 3D numerical model of [24], which again does not capture the internal structure.

There is a parallel line of research focusing on the modelling of branching structures in the field of mineral dendrites, which also takes inspiration from DLA processes [26, 27]. Recent work using Lattice Boltzmann methods to simulate the formation of mineral dendritic structures [28] shares some similarities with the gross morphologies produced by our model in the branched growth regime, highlighting the potential similarities of biotic and abiotic processes.

3 Proposed Model

3.1 Goals of the Model

The goals of the model presented are to capture the range of morphologies present across the spectrum of microbialites (and potentially abiotic morphologies) within a generic, parsimonious framework. This model is intended as a starting point for the resumption of agent-based modelling of microbialite formation, leaving scope for extensibility or specialisation.

We do not claim or attempt to capture the full range of physics, biology and chemistry underlying the multitude of interacting processes that affect the formation and preservation of microbialites. However, our model is intended as a conceptual and exploratory tool, providing a step forward compared to previous work and building on technological developments that make it worthwhile to return to this topic. The model necessarily contains a large number of parameters; we detail these in the SI.

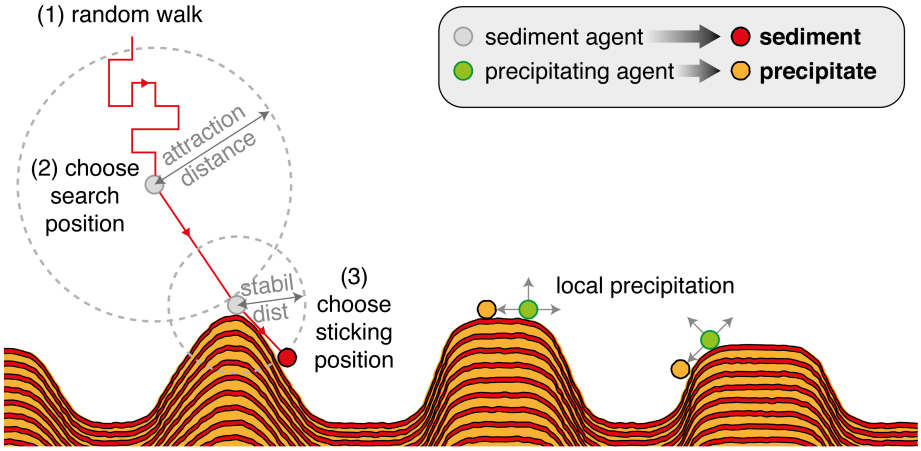

Figure 1. Schematic overview of the model showing the dynamics of each agent type. Figure inspired by Dupraz, Pattisina, and Verrecchia [17].

3.2 Modelling Framework

In this work, we use the `Agents.jl` [29] agent-based open source modelling framework. We chose this approach for several reasons. First, `Julia` is an accessible high-performance programming language. Second, such a framework allows us to focus on the dynamic rules implemented rather than the details of the ABM implementation, which are handled and optimised by the framework. Third, the choice of `Julia` and `Agents.jl` aids extensibility as all the underlying code is pure `Julia`, simplifying the process of modifying the model with fast user-friendly code. Finally, this framework supports parallel computing; parallel simulations can initialised in a few lines on a laptop, making it well-suited for exploring large morphological parameter spaces. Additionally, the framework can be utilised to run the model interactively, allowing live parameter exploration.

3.3 Set-up of the model

The model simulates the formation of a two-dimensional microbialite, drawing inspiration from the model of [17], using a grid with periodic horizontal boundary conditions. Extensions to three dimensions could be considered in future work (and would be simplified by the `Agents.jl` framework). Our model consists of two separate processes, each represented by a distinct set of agents. One group of agents represents sediment particles that are trapped and bound due to "microbial activity" on the surface of a solid substrate. The other group comprises precipitating agents that reside at the solid–fluid interface and represent an active microbial layer that can induce mineral precipitation. We do not attempt to simulate the detailed dynamics of the biofilm; instead, we focus on the events of precipitation and sedimentation (trapping and binding), as these dominate the features most likely to be preserved in the geological record and observed in fossil microbialites.

Each agent or grid cell does not represent an individual sediment grain or microbe, but instead the aggregate effects of a collection of processes at a larger scale. Each agent type can fill cells of the grid, leading to growth in the solid structure. When each agent type fills a cell this is marked with a distinct value, allowing for clear differentiation between precipitated and sediment-derived material when visualised as colours. The different values can be taken to represent some physical property (e.g. grain size) or chemical characteristics (e.g. mineralogy or elemental composition) that would allow sediment and precipitate to be differentiated via petrographic techniques or elemental mapping such as energy-dispersive X-ray spectroscopy (EDX) [30]. In this work, we plot microbially induced precipitation in yellow and trapped/bound sediment in red. Distances between cells in the model are measured using the euclidean distance function in `Agents.jl`.

3.4 Sediment Agents

The dynamics of sediment agents draws from the work of [17] and hence the physics of diffusion-limited aggregation. At each time-step, a given number of sediment agents are introduced to the simulation. These agents are given two agent-level properties that impact the morphology: the stability distance and the attraction distance. A sediment agent which has not yet attached to the solid structure will look for locations, directly adjacent to solid filled cells, within its attraction distance radius to conduct a stability search from. The agent sequentially selects the locations from the randomly shuffled list within the attraction distance for a stability distance search until successful. See schematic, figure 1.

During the stability search within its stability distance, the agent looks for a valid and preferred location to "stick"and fill a cell with labelled solid. A location is valid if it is currently empty and has at least one neighbouring solid-filled cell. From valid locations, the sticking site is selected stochastically. The probability of sticking at site i is given by:

$$p_i^{stick} = \frac{\nu_i}{\sum_j \nu_j}, \tag{1}$$

where the sum of cells in the denominator runs over all valid locations, and ν_i is the number of solid neighbours for a given candidate cell.

This formulation gives preference to sites that are more structurally stable, adjacent to more solid material. If the agent sticks successfully, this grid cell is marked as solid sediment, and the agent is removed from the simulation. With a given recolonisation probability, the site of the newly stuck agent can acquire a precipitating agent, representing microbial activity, which can initiate local

mineral precipitation. If no places to stick are found, the agent undergoes a biased random walk with equal probability of moving left or right at given horizontal speed and biased probability, 90% chance, of moving down rather than up at a given vertical speed, to force downwards motion with a small amount of randomness. The walk function uses fixed step sizes, and the agent cannot walk into other agents, as we enforce one agent per cell. If a sediment agent hits the bottom of the grid or walks into the solid, it is removed from the simulation. The walk function could be modified to introduce directional bias (e.g. simulating flow or current without full hydrodynamic simulation) or made time-dependent to simulate environmental conditions.

3.5 Precipitating Agents

Precipitating agents can either be introduced by the growth of another precipitating agent, through recolonisation triggered by a sediment agent sticking, or by the setup of the initial conditions. At the start of each step, precipitating agents may be removed with a given probability to simulate random processes that could interfere with agents (e.g., grazing, metabolic shutdown, or erosion). If the agent remains, it loops over each of its immediate neighbouring cells (in a given metric, which includes diagonals for euclidean), selects the empty cells, and assigns each of these cells a weight, w_i, indexed from a parameter array, depending on whether it is up, down, or horizontal relative to the cell. A cell is then selected for potential growth with probability

$$p_i^{\text{grow}} = \frac{w_i}{\sum_j w_j}, \tag{2}$$

where the denominator of the fraction is a sum over all valid growth directions. Growth to the selected cell then occurs stochastically according to the current value of the precipitation probability. When an agent grows, it fills the selected cell with labelled solid and creates a precipitating agent at that location. Finally, precipitating agents that become completely surrounded by solid-filled cells are removed from the simulation, mimicking the smothering of microbial mats.

3.6 Initial Setup

We use `Agents.jl` to initialise a model and select a random scheduler, to prevent sequencing artifacts. The model starts with an initial solid substrate, labelled distinctly from either sediment or precipitate. This initial substrate can be of any shape. However, we limit it to five configurations in this work: a single flat horizontal layer, a localised horizontal patch, a small mound, a small triangle or sinusoidal fluctuations all along the base of the model. Onto this solid substrate, we place precipitating agents with a probability according to the defined initial density, details given in the SI.

3.7 Periodicity and Sediment Addition

In order to grow the structure, we introduce sedimenting agents over time as they are continually depleted when forming the solid. In previous work [17], sedimentation was generally introduced at a constant rate. However, this does not need to be the case, as periodic sedimentation can be incorporated into the model. Moreover, independently of any periodicity in the sedimentation, there may be externally forced periodicity in the rate of microbial induced precipitation. The varying strength of either of these sources of periodicity, or the interaction between them both,

may parsimoniously explain the emergence of the varied internal structures of microbialites. In physical terms, periodicity may occur in microbial activity, carbonate concentrations, background sediment rate or almost any other environmental process likely to modify the rates of precipitation or trapping and binding on any appropriate time scale (daily, weekly, seasonally, etc.).

In our model, to minimise as much as possible the number of parameters, we modulate the precipitation rate and the sediment rate in the following way. We set the sediment rate equal to

$$\text{sediment rate} = \text{round}(A_{\text{sediment}} f_{\text{s}}(\frac{2\pi t}{T})). \tag{3}$$

Where A_{sediment} is the maximum sediment rate or sediment amplitude and T is defined as the period control parameter. We also round the sediment rate as we can not add a non-integer amount of sediment. The modulation $f(\frac{2\pi t}{T})$ can be any function that takes values $[0, 1]$ and depends on the number of time-steps passed, t. In order to reduce the number of parameters, in this study we couple the modulation of the precipitation rate to the modulation of the sediment rate (although they could be decoupled in future work). The precipitation rate is defined as

$$\text{Precipitation Probability} = A_{\text{precipitation}} f_{\text{p}}(\frac{2\pi(t + b_{\text{offset}})}{a_{\text{scale}} T}). \tag{4}$$

Where repeated parameters are as in the sediment rate definition (equation 3), $A_{\text{precipitation}}$ is the maximum precipitation rate or precipitation amplitude, which is a probability $[0, 1]$. While b_{offset} and a_{scale} set the way two mechanisms interact.

We allow independent modulation functions, f_p and f_s, for the precipitation rate or the sediment addition rate to be chosen from the following options in addition to constant behaviour: $\max(\cos x, 0)$, $\cos^2 x$, or $|\cos x|$. Hence, we refer to T as a "period control parameter" as when changing functions and scaling etc. it may no longer be the true period but will simply act as a related control parameter. Due to the generality of the model, any parameter can be made time-dependent and updated according to any function (periodic or not), which respects the constraints of the model dynamics. For simplicity, in this work we largely set the periodic function to $\max(\cos x, 0)$, as it most clearly promotes layer formation. However, we find that lamination can still emerge using other functional forms.

For each given sedimentation rate, we add sediment agents into the grid by the following process. Rather than releasing all agents at the top of the grid, we release from a lower height for computational efficiency, with the addition of some randomness to prevent computational artifacts. Then, we select a set of possible input locations by several steps. Firstly, we determine the base input row as the minimum between the height of the grid minus 5 and the maximum height of the solid plus 10 times the vertical step size. A random downward offset of between 1 and the step size minus 1, is applied to this base row. Secondly, using this base row, we select all valid locations, not already solid or containing an agent, across all columns and ±5 rows in either direction. Finally, from this set of possible locations, we randomly draw (without replacement) until we have added the required number of sediment agents.

3.8 Overview of Model

This model separates sedimentation (trapping and binding) from microbially induced precipitation, giving more insight into emergent morphology and allowing more hypotheses to be tested. Due to the nature of agent-based modelling, there are a large number of parameters and some choices

that need to be made by the modeller, which are arbitrary within the realm of reasonableness, such as how exactly to select the release height positions. This model is also not necessarily unique in that there are likely other ways to simulate the microbialite formation process. However, this work provides a principled starting point, linking back to previous approaches [17].

It is important to note that the current model works only in simulation units, rather than being connected directly to physical time or space. Linking a model of this kind to physical units may be the subject of future work. However, it is difficult to precisely calibrate against the growth rates of real world microbialites, while aspects of the morphological patterns generated by DLA are scale-invariant by nature [31]. When running the model, we impose a maximum number of time steps or in the case of visualisation and morphospace plots stop the run when the maximum height of the structure reaches within 50 cells of the top of the domain.

4 Results

4.1 Comparison to Real Microbialites

Microbialites exhibit a remarkable diversity of forms, shaped by the interplay of environmental conditions and microbial processes over various timescales [3, 6]. Although the full morphological spectrum cannot be fully captured in just a few figures, we present a curated selection of representative examples (figure 2), from different geological periods, that highlight key structural characteristics observed in the field. These comparisons serve as qualitative targets for our simulations, and we demonstrate that our model is capable of reproducing a broad range of these morphologies under different parameter settings.

Our simulation does not aim to replicate these structures at the microscopic level or reflect precise growth mechanisms. However, our ability to approximate such diverse morphologies with a limited number of adjustable parameters demonstrates the explanatory power of the model. This approach bridges the gap between field observations and generative modelling, offering a conceptual framework to explore how environmental and microbial controls may shape microbialite architecture across geological time.

In figure 2, we show how our model qualitatively reproduces a range of microbialites with laminations arising from the interplay between the agent types in the model. One caveat with this approach is that the real object is three-dimensional whereas the images show two-dimensional slices. This creates geometric artifacts that can modify the appearance of branches, which are difficult to replicate in a two-dimensional model. Parameters of the reproductions are listed in the SI.

4.2 Exploring the Parameter Morphospaces

One way to elucidate the behaviour of the model is to plot the generated structures into a morphospace. As there are many control parameters for this simulation, we cannot plot them all simultaneously in a way that can visualised. However, in figure 3 we show a subset of key parameters that most strongly influence the emergent external morphology.

Specifically, we explore the effect of varying two of attraction distance, stability distance, and precipitation amplitude at a time, while holding all other parameters constant (see SI for values). We show simulations under both localised and uniform initial conditions to highlight how the initial setup interacts with model dynamics to shape the final structures.

(**a**) Stromatolite from the Goose Egg Formation, Wyoming, USA (ca. 250 Ma), featuring large, laterally extensive domes with relatively flat lamination

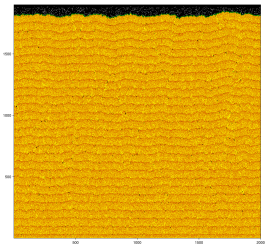

(**b**) Simulated version of (a)

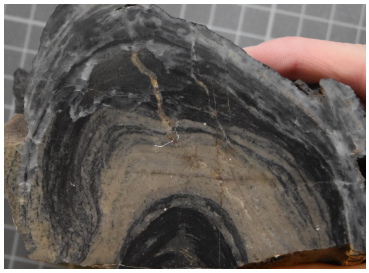

(**c**) Stromatolite from the Campbellrand-Malmani Subgroup, South Africa (ca. 2.5 Ga), showing small laminated domes

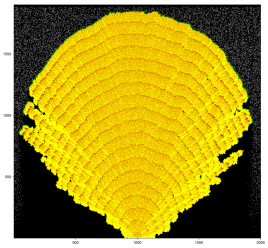

(**d**) Simulated version of (c)

(**e**) Linked-columnar stromatolite from the El Molino Formation, Potosí, Bolivia (ca. 70 Ma), characterized by fine columns with continuous laminae

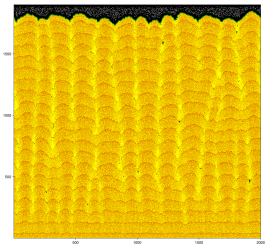

(**f**) Simulated version of (e)

(**g**) Domical microbialite branching into long dendritic columns from the Howe Limestone Member, Kansas, USA (ca. 295 Ma).

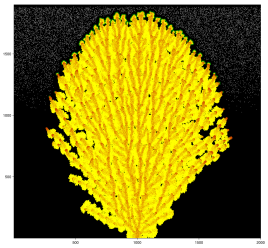

(**h**) Simulated version of (g)

Figure 2. Comparison of real microbialite specimens (left column) and simulated analogues produced by our agent-based model (right column), under distinct parameters. In simulation panels, precipitation is shown in yellow and sediment in red. All parameters listed in the SI.

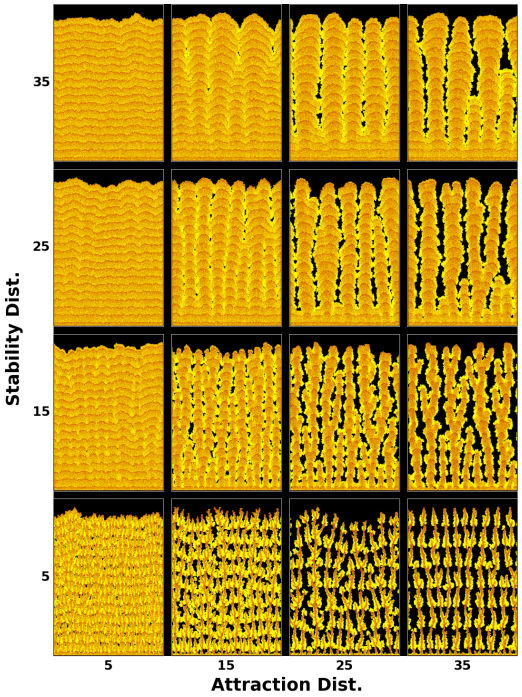

(**a**) Attraction Distance and Stability Distance

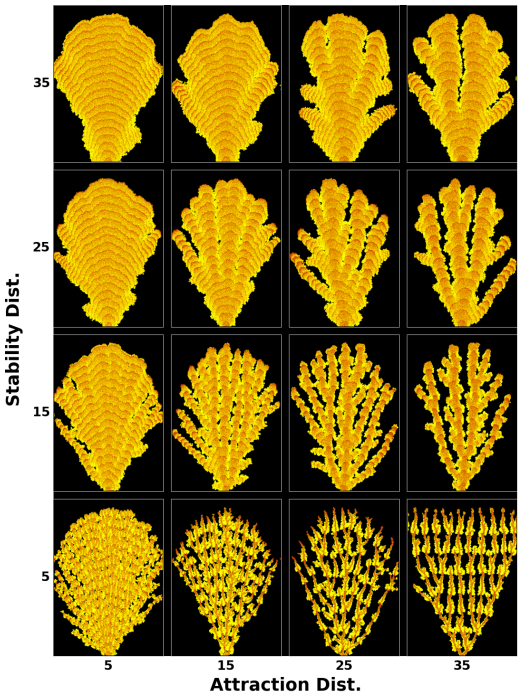

(**b**) Attraction Distance and Stability Distance with Localised Initial Conditions

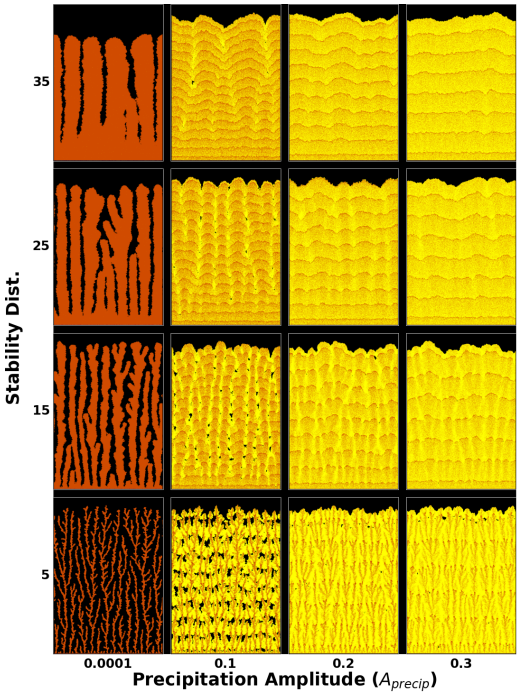

(**c**) Precipitation Amplitude and Stability Distance

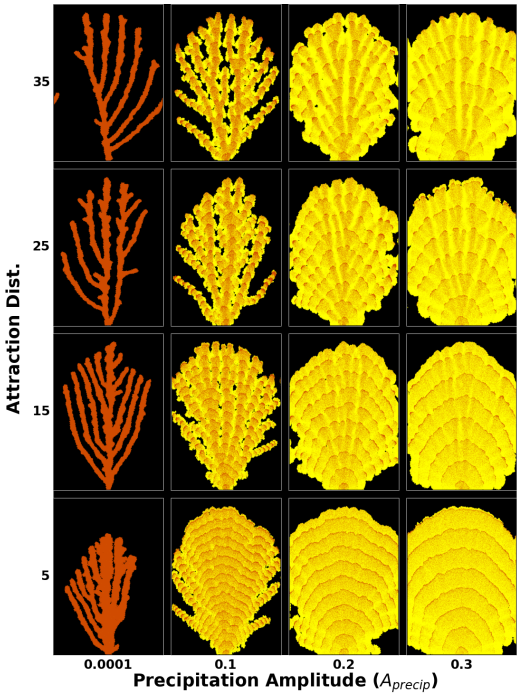

(**d**) Precipitation Amplitude and Attraction Distance with Localised Initial Conditions

Figure 3. Parameter Morphospaces. Demonstration of the wide range of possible morphologies generated and the parameter dependence. Precipitation in yellow, sediment in red. Parameters in SI.

The first morphospaces (figures 3a, 3b) show how the stability distance and the attraction distance control the output morphology. High stability distance combined with low attraction distance leads to flatter layered structures. High stability distance combined with high attraction distance leads to columnar structures. Low stability distance combined with high attraction distances leads to sparse branching structures. Low stability combined with low attraction distance leads to smaller scale branching which is partially overwhelmed by mineral precipitation, in this example.

Our results mirror those of [17] figure 3, where similar trends are observed, albeit at different scales. Figures 3b, 3d show the impact of spatially localised initial conditions and how this directly leads to radial or domal morphologies as the structure grows from a central point. This is important as many real-world microbialites have this morphology and growth from a localised nucleus provides a parsimonious explanation for this.

Figures 3c, 3d show how changing the rate of microbially induced precipitation leads to variations in morphology. Very low precipitation rates lead to DLA-like morphologies without layering. At sufficient growth rates, regular layers can appear, alternating between sediment- and precipitate-dominated phases, with layer thickness depending on the periodicity and balance of the two parameters. Internal branching or clotted patterns can also be maintained as the structure grows. All of these reflect the possible diversity of internal structure of microbialites and demonstrate the interactions between external and internal processes.

4.3 Interactivity and Abrupt Morphological Transitions

The parameters that govern the formation of real microbialites may not be constant throughout the development of the structure, either gradually varying or suddenly changing. Any parameters in this model can be made time-dependent by updating the values during each time step according to any function or rule. However, this leads to an explosion of possibilities that could be tested and structures that may emerge. In order to address this and additionally make the work more accessible, we include an interactive simulation using `Agents.jl` [29] and the `abmexploration` function. This version allows the simulation to launch in an interactive window, where a user can watch as the simulation progresses, as well as update the values of selected parameters, live as the simulation runs, using sliders. This can be accessed by running the code included in the supplementary materials. In the supplementary material, we include several videos of this in progress. A guide on how to run and install the code is given in the SI.

This feature allows insight into how parameter variations can lead to a whole range of structures, and could also be used as a teaching aid demonstrating theories of microbialite formation. Recognising this complexity is crucial when reconstructing paleoenvironmental conditions from fossil microbialites. Parameter variation during runs was shown in the work of Dupraz, Pattisina, and Verrecchia [17]. However, our model includes internal fabrics and allows the user to see intuitively how they emerge from various parameters.

4.4 Decoupling Internal and External Morphologies

A key step forward in this work is the ability to generate a variety of internal structures and external morphologies as the simulated microbialite grows. This allows us to illustrate the complexity and contingency of microbialite formation and classification. Figure 5, illustrates how the approximate external morphology can be maintained while the internal structure radically changes. This is done

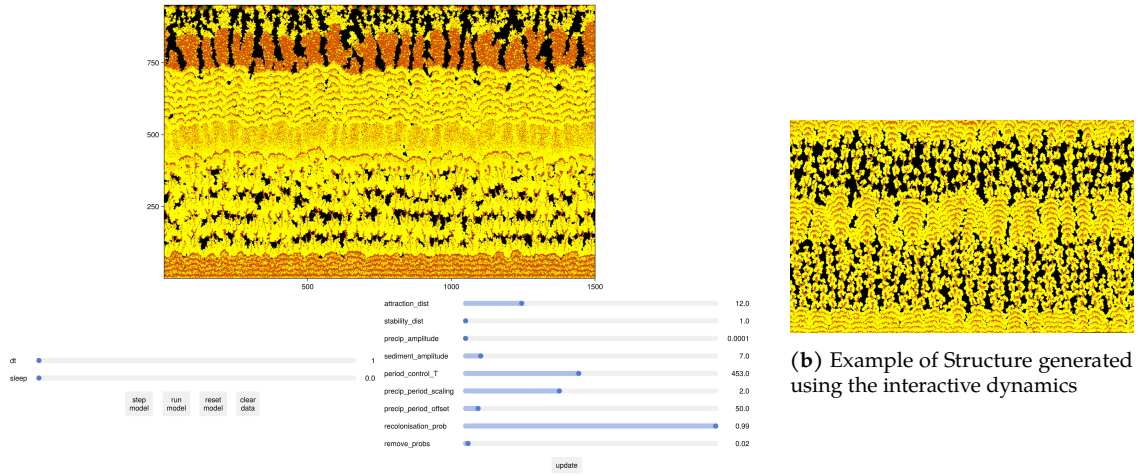

(**a**) Interactive Interface

(**b**) Example of Structure generated using the interactive dynamics

Figure 4. Interactive Interface and Morphological Transitions. (a) Screenshot of the Interactive Interface showing sliders which allow parameters to modified during the run and an example structure created by this process. (b) Simulated structure with abrupt morphological changes generated by abrupt parameter changes using the interactive mode.

by varying the period control parameter that influences the emergence of stromatolite, dendrolite, leiolite, or thrombolite internal fabrics.

For various values of stability and attraction distances, figure 5, we plot the changes in morphology that occur when varying the periodicity control parameter. As we change the periodicity control parameter, we see a transition between discrete layers and the breakdown of lamination into random noise via clotting. This suggests that the magnitude of external periodic forcing governs a spectrum of internal fabrics from leiolites to thrombolites and stromatolites. Changing the external periodicity also modifies the rate at which material accumulates so that during near-constant precipitation the intercolumnar spaces are filled with precipitate. This demonstration, figure 5, suggests a degree of equifinality in microbialite form: different combinations of parameters can produce similar final forms, potentially limiting or complicating efforts to use microbialites as "environmental dipsticks". The decoupling of internal and external morphologies suggests that the combination may give greater insight into the formation mechanism than one alone. Laminations give more information about the growth history of a microbialite than amorphous randomness, which may be more difficult to interpret. Additionally, in reality, a real object is only observed when dynamics have ceased, making it difficult to separate rate, speed, and time uniquely depending on how laminations may or may not record the evolutionary history

4.5 Additional Model Features

4.5.1 Quantitive Measurements, Parameter Sweeps and Equifinality

Another useful aspect of this model is the ability to quantitively characterise the resulting structure, either aggregating or separating the two processes. A huge number of potential summary statistics

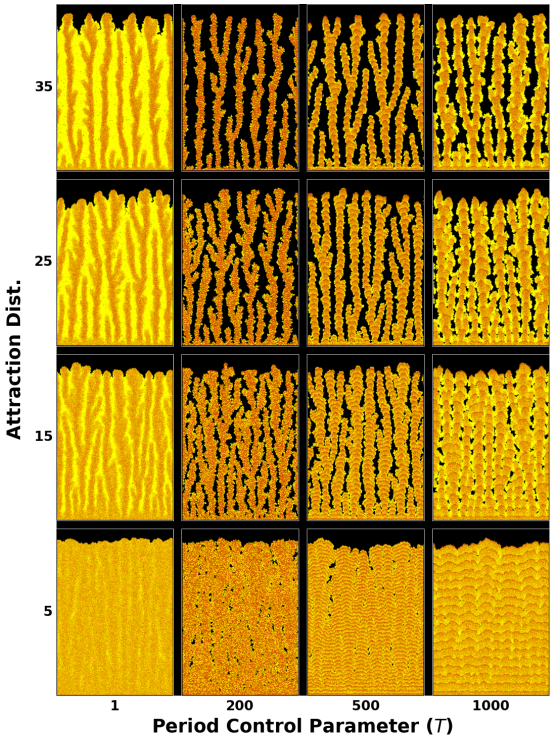

(**a**) Period Control Parameter and Attraction Distance

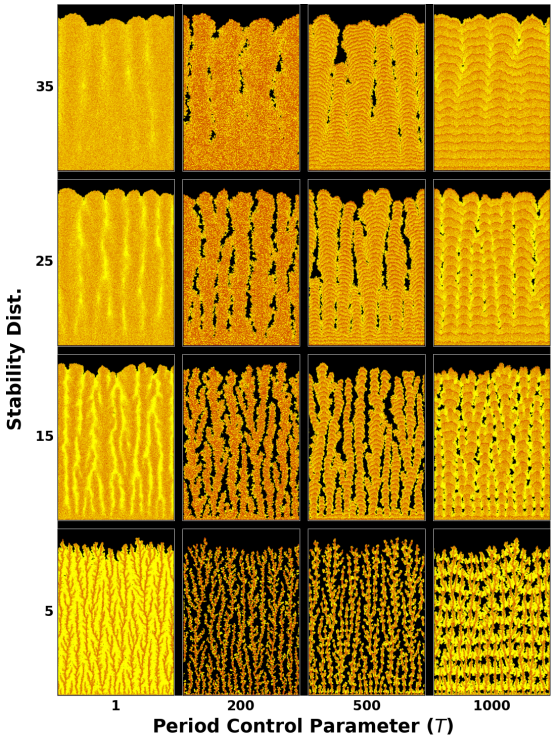

(**b**) Period Control Parameter and Stability Distance

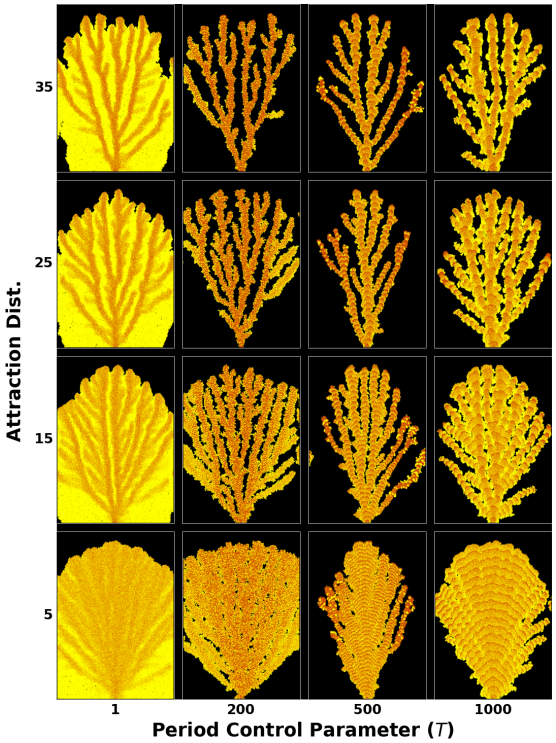

(**c**) Period Control Parameter and Attraction Distance (Localised Initial Conditions)

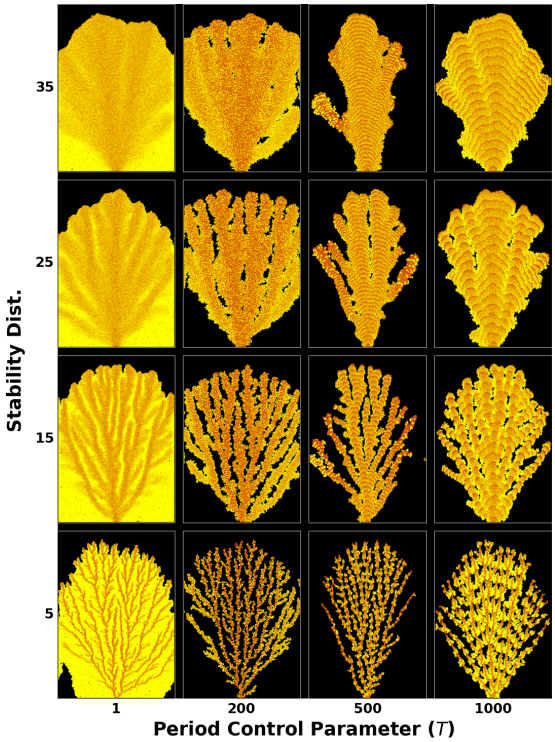

(**d**) Period Control Parameter and Stability Distance(Localised Initial Conditions)

Figure 5. Internal Fabric Transitions: Variations in internal Morphology with changes in external periodic control demonstrating transitions between microbialite types in several morphospaces

could be used to describe the model outputs. In the SI, we give examples of some of these measures, and how they correlate with the input parameters and each other. Our framework makes it relatively simple to run independent simulations in parallel using high-level `Julia` multithreading. This speeds up the sampling of the parameter space. However, there are still a large number of variables that could contribute. In order to simplify the process, we use Latin hypercube sampling, which allows the samples to be evenly distributed across parameter space while controlling the number of samples, and focus on the key parameters of stability distance, attraction distance and precipitation rate. One key conclusion of this analysis is the suppressive nature of certain parameters. Different strengths of correlations can be observed depending on the inclusion of precipitation rate in the sweep; if this is too large, it can dominate the structure and hide other affects.

Quantitative analysis reveals two subtly different types of equifinality. Firstly, parameter-dominance equifinality occurs once a regime is reached where one parameter, such as precipitation rate, dominates, and this can obscure effects of other more subtle parameters. Secondly, a type of measurement equifinality is observed if a structure is summarised by a particular measurement; it is possible for simulated microbialtes with very different internal structures to have similar values of some measurements, or for measurements to be insensitive to parameter changes until a phase transition occurs in the output. Strong absolute equifinality, where distinct parameter sets give exactly identical outputs, has thus far not been found in this model, due to the complexity of the parameter space, the interactions within it, and the stochasticity of the model. One may anticipate that by halving one parameter and doubling another, or some conceptually equivalent action, it would be possible to create a structure which is absolutely identical to the original, but this is not something we observe despite some effort to search for it.

Figure 6, details how these observations play out. Figure 6a shows how increasing precipitation amplitude leads to a regime where surface roughness is suppressed and structures merge together, with figures 6b and 6c showing how a large change in attraction distance makes only a small contribution to the final outcome in this regime.

We can also demonstrate measurement equifinality in figures 6d, 6e and 6f where we see two examples of two structures that have almost identical mean fractions of each row filled. This parameter (which can successfully detect the emergence of columns and branching) is insensitive to the difference between flat laminations and the "almost" splitting columns. This could be avoided by choosing different measurements, but the key point is that reducing the structure to a set of measurements inevitably loses information. Hence, relying only on quantitative measurements can miss important nuances.

This result has implications for biogenicity assessment using quantitative measurements. Care must be taken to ensure that the chosen measurements adequately capture the nuances of the structure. Moreover, biogenicity determination using methods that depend heavily on a single parameter are vulnerable if other factors can hide the effects of that parameter.

5 Discussion

5.1 Extensibility

As this is a high-level minimal model, there are vastly many possible extensions to this work. We include the heuristic conical-like stromatolite morphospace, in the SI, to show the ease of adding extensions, while also highlighting the additional complexity and parameter creep that may occur. To reduce complexity in this study, we deliberately omit additional factors, such as a rising tide

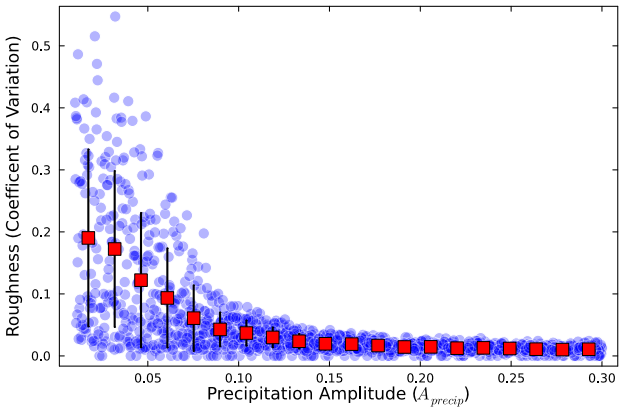

(**a**) Surface Roughness as function of precipitation amplitude while sampling precipitation amplitude, stability distance and attraction distance

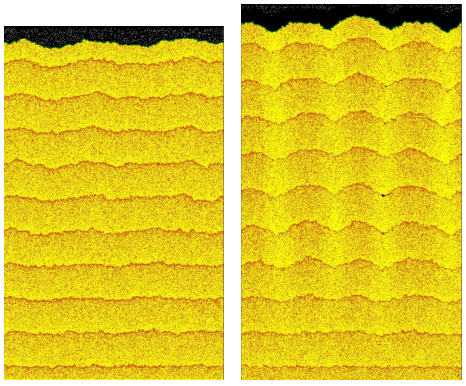

(**b**) High Stability Distance, Low Attraction Distance, High Precipitation

(**c**) High Stability Distance, High Attraction Distance, High Precipitation

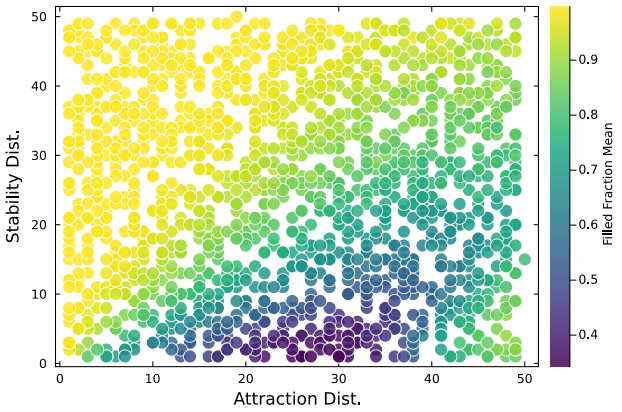

(**d**) Mean Filled Fraction while varying stability and attraction distance and fixing precipitation amplitude

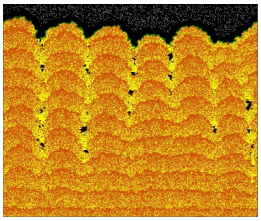

(**e**) "Almost" Disconnected Columns

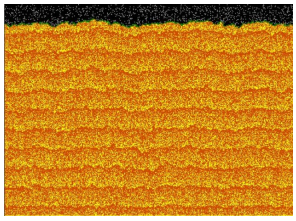

(**f**) Simple Flat Laminations

Figure 6. Quantitative Measurements and Equifinality (a) suppression of surface roughness and detail by increasing precipitation (b),(c) demonstrate how distinct columns what would be created by attraction distance are merged in this regime (d) Shows variations in mean filled fraction across parameter space (e),(f) nuances of structure that can be missed by this measurement

of background sedimentation, which could interact with the structure, as this would complicate our morphological measurements and increase parameters further. However, incorporating such processes may be necessary to simulate certain microbialite formation scenarios more accurately, particularly those where environmental sedimentation plays a dominant role.

A natural extension of the current model is to implement it in three dimensions, as true microbialites are inherently three dimensional objects and there may structures that depend on the fact that they exist in three dimensions, as illustrated by [24] in one particular context. This would require a relatively minor update to the simulation logic, although changing the dimension may affect the type of DLA structures formed. Extensions to three dimensions could be accompanied by implementation of more realistic hydrodynamics, to show the roles that currents and tides may play in the formation of microbialites. This would require solving for the fluid velocity field given the morphology and boundary conditions and advecting the sediment according to this. This could also dovetail with implementation of erosion and scouring dynamics to modify the structure over time in response to fluid flow, an important factor in microbialite preservation and morphology.

Other disruptions of the structure could also be added, such as gas bubbling, physical disturbance of the mat by other organisms, or slumping due to mechanical instability. A range of modifications could be made to move beyond the simple DLA model of the sediment dynamics to incorporate more realistic sediment behaviour and intra-sediment interactions (e.g., capturing sediment angle of repose). Furthermore, the growth dynamics could be replaced with a more realistic model of the drivers of microbial induced precipitation, simulating the microbial metabolic pathways (e.g., photosynthesis, sulfate reduction) that drive changes in local geochemistry. Finally, real microbialites are often significantly altered during diagenesis, with potential overprinting of their primary structure. A future extension of the model could incorporate a simplified diagenetic filter to approximate post-depositional changes such as recrystallization, compaction, or cementation, further bridging the gap between simulation and observed field structures.

Another modification which could be made is to introduce a structured temporal variation to the parameters beyond what can be done with the interactive simulation. This could reflect a variety of variations in the local environment (such as tidal cycles, seasonal changes, hydrothermal pulses or changing microbial community composition). Such temporal variation is a suspected driver of the structure of real microbialites [7, 32, 33]. We could also incorporate additional classes of sediment or precipitate, which may have different dynamics and interactions. These could represent, for example, varying grain sizes, mineralogies (e.g., carbonates vs. sulfates) or biologically vs. abiotically mediated phases. By assigning separate labels to each class, the resulting composite structures could encode more complex physical or chemical heterogeneity.

This model is presented at an opportune time. We expect that agentic AI will excel at building variants of this model from the starting point and high-level code framework offered in this study.

5.2 Implications for Biogenicity and Inference of Generative Process

It is well-understood that morphology alone is an ambiguous indicator of biogenicity [8, 34]. Our model demonstrates how relatively simple mechanisms, when properly arranged, can lead to a wide diversity of microbialite morphologies. This supports the claim that morphology is ambiguous in the following way: In our model, the parameters are an abstraction of the underlying processes. From the perspective of the model it does not matter what causes a particular parameter value or even what substance the sediment and precipitate represent. This implies that a given morphology could be the result of a range of biological or abiotic processes or some combination of the two. This is a form

of "external equifinality" where the morphology is the result of simple interacting processes based on few parameters; however, the parameters are the result of potentially wide-ranging mechanisms.

Hence, a principled extension of this work would be to explore how models of this type (or extensions) could also simulate abiotic structures that are similar in morphologies to microbialites such as the "paint stromatolites" of McLoughlin, Wilson, and Brasier [35] or the formation of wind-driven digitate sinter structures [36] similar to objects observed on Mars [11].

This work implies that multiple, distinct physical or biological processes may be effectively captured by the same simple mechanism, reinforcing the idea that morphology, while informative, is not sufficient on its own to resolve biogenicity without further contextual or geochemical evidence.

5.3 Further Discussion

In this work, we focus on a subset of the most influential and directly interpretable parameters, selected for their relevance to previous literature [17]. Of course, there is a whole range of behaviour that may be extracted from varying other parameters; however, we limited our scope to a concise set in order to maintain clarity and interpretability. The model presented here does not provide a detailed account of every aspect of microbialite formation, but complements the existing literature by emphasising the need for models to consider internal structure and rekindling agent-based approaches in this field. Even in its most simplified form, it is crucial that models try to move beyond gross morphology and begin addressing internal layering and composition.

A key assumption of this work is that the layering results from a fixed external periodicity, such as seasonal or climatic cycles. This simple assumption reflects hypotheses in the stromatolite literature [7, 32, 33]. For conciseness, we focus on morphology and broad internal fabric categories. However, the origin of laminations and the nature of periodic structures observed in stromatolites are fundamental questions. Hence, we plan to dedicate a future follow-up paper solely to addressing these questions.

One of the key contributions of this work is accessibility. The code for this model is written in a high-level, open-source framework that ensures both ease of use and computational efficiency, thus lowering the barrier to entry for further development and experimentation. Additionally, we offer the first interactive simulation tool allows intuition to be gained into structure formation, hypothesis to be formulated and serves a potential outreach or teaching aid.

Further extensions may include more direct links to real microbialites. This could include testing hypotheses related to the driving forces in the formation of specific structures. It would also be worthwhile to relate the quantitative metrics used to describe the structures in this work to those commonly applied in field-based and image-based studies of microbialites. A key step would be to link the model parameters to real-world variables and add physical units to the simulation. However, this presents a significant challenge, as the simulation parameters are an aggregate of many factors, and DLA leads to self-similar behaviour. There is also the additional issue that a given layer thickness is both a function of growth rate and the time it was allowed to grow, with both needing to be constrained simultaneously.

6 Conclusion

We have presented an agent-based model of microbialite formation which produces for the first time a wide range of morphologies, both internal and external, while being accessible interactively. This model demonstrates that diverse morphologies can originate from simple rules coupled to

external periodicity explaining the ambiguity and non-uniqueness of morphology as many process biotic or abiotic may map to these rules. We also highlight how this setup can be used to study the output quantitatively, and raise the broad possibilities of extensions, one of which we demonstrate via a conical heuristic in the SI. Although deliberately abstracted and high-level, our model captures essential aspects of microbialite morphogenesis and highlights the value of agent-based approaches to explore structure–process relationships. We hope that this model provides a useful resource and impetus for renewed efforts in the modelling of microbialite formation, ultimately leading to a better understanding of the role of biology in their formation and how this can be distinguished from abiotic processes.

Data Availability

All data, including images of all quantitive sweep microbialites and videos of dynamics, the code and instructions for how to run the interactive model can be found at `https://github.com/nrodgers1/Microbialite_simulator`. This will be deposited in a permanent repository upon acceptance.

Funding

The authors acknowledge the support of the Human Frontier Science Program under grant number RGP006/2024.

Declaration of Interests

The authors declare no conflict of interest.

References

[1] R. V. Burne and L. S. Moore. "Microbialites: organosedimentary deposits of benthic microbial communities". In: *Palaios* (1987), pp. 241–254. DOI: 10.2307/3514674.

[2] R. E. Riding and S. M. Awramik. *Microbial sediments*. Springer Berlin, Heidelberg, 2000. DOI: 10.1007/978-3-662-04036-2.

[3] K. Grey and S. M. Awramik. "Handbook for the study and description of microbialites". In: *Geological Survey of Western Australia Bulletin* 147 (2020).

[4] M. J. Van Kranendonk et al. "Geological setting of Earth's oldest fossils in the ca. 3.5 Ga Dresser formation, Pilbara Craton, Western Australia". In: *Precambrian Research* 167.1-2 (2008), pp. 93–124. DOI: 10.1016/j.precamres.2008.07.003.

[5] K. Hickman-Lewis et al. "Most ancient evidence for life in the Barberton greenstone belt: Microbial mats and biofabrics of the 3.47 Ga Middle Marker horizon". In: *Precambrian Research* 312 (2018), pp. 45–67. DOI: 10.1016/j.precamres.2018.04.007.

[6] L. Fogret, P. Sansjofre, and S. V. Lalonde. "Geochemistry of carbonate microbialites through time and space: Insights from the microbialite collection of the Muséum National d'Histoire Naturelle (MNHN), France". In: *Chemical Geology* 662 (2024), p. 122239. DOI: 10.1016/j.chemgeo.2024.122239.

[7] R. P. Reid et al. "Microbialite accretion and growth: lessons from Shark Bay and the Bahamas". In: *Annual review of marine science* 16.1 (2024), pp. 487–511. DOI: 10.1146/annurev-marine-021423-124637.

[8] J. M. García Ruiz et al. "Morphology: an ambiguous indicator of biogenicity". In: *Astrobiology* 2.3 (2002), pp. 353–369. DOI: 10.1089/153110702762027925.

[9] M. J. Van Kranendonk et al. "A review of 3.7 Ga stromatolites from the Isua Supracrustal Belt, West Greenland". In: *Earth-Science Reviews* 262 (2025), p. 105034. DOI: 10.1016/j.earscirev.2024.105034.

[10] A. P. Nutman et al. "Rapid emergence of life shown by discovery of 3,700-million-year-old microbial structures". In: *Nature* 537.7621 (2016). ISSN: 14764687. DOI: 10.1038/nature19355.

[11] S. W. Ruff and J. D. Farmer. "Silica deposits on Mars with features resembling hot spring biosignatures at El Tatio in Chile". In: *Nature Communications* 7 (2016). ISSN: 20411723. DOI: 10.1038/ncomms13554.

[12] C. Dupraz et al. "Stromatolitic knobs in Storr's Lake (San Salvador, Bahamas): A model system for formation and alteration of laminae". In: *Geobiology* 11.6 (2013). ISSN: 14724677. DOI: 10.1111/gbi.12063.

[13] M. T. Batchelor et al. "Deterministic KPZ model for stromatolite laminae". In: *Physica A: Statistical Mechanics and its Applications* 282.1 (2000). ISSN: 03784371. DOI: 10.1016/S0378-4371(00)00077-7.

[14] M. Batchelor et al. "A case for biotic morphogenesis of coniform stromatolites". In: *Physica A: Statistical Mechanics and its Applications* 337.1-2 (June 2004), pp. 319–326. ISSN: 03784371. DOI: 10.1016/j.physa.2004.01.065.

[15] M. Batchelor et al. "Statistical physics and stromatolite growth: new perspectives on an ancient dilemma". In: *Physica A: Statistical Mechanics and its Applications* 350.1 (May 2005), pp. 6–11. ISSN: 03784371. DOI: 10.1016/j.physa.2005.01.014.

[16] R. Cuerno et al. "Pattern formation in stromatolites: Insights from mathematical modelling". In: *Journal of the Royal Society Interface* 9.70 (May 2012), pp. 1051–1062. ISSN: 17425662. DOI: 10.1098/rsif.2011.0516.

[17] C. Dupraz, R. Pattisina, and E. Verrecchia. "Translation of energy into morphology: Simulation of stromatolite morphospace using a stochastic model". In: *Sedimentary Geology* 185.3-4 (Mar. 2006), pp. 185–203. ISSN: 00370738. DOI: 10.1016/j.sedgeo.2005.12.012.

[18] H. J. Hofmann. "Attributes of Stromatolites". In: *Geological Survey of Canada* (1969), pp. 69–39. DOI: 10.4095/106437. URL: https://doi.org/10.4095/106437.

[19] T. Bosak, A. H. Knoll, and A. P. Petroff. "The meaning of stromatolites". In: *Annual Review of Earth and Planetary Sciences* 41 (2013). ISSN: 00846597. DOI: 10.1146/annurev-earth-042711-105327.

[20] J. P. Grotzinger and D. H. Rothman. "An abiotic model for stromatolite morphogenesis". In: *Nature* 383.6599 (1996). ISSN: 00280836. DOI: 10.1038/383423a0.

[21] A. P. Petroff et al. “Biofilm Growth and Fossil Form”. In: *Physical Review X* 3.4 (Nov. 2013), p. 041012. ISSN: 2160-3308. DOI: 10.1103/PhysRevX.3.041012.

[22] G. W. Ojakangas, S. M. Awramik, and M. C. Storrie-Lombardi. “Stromatolite photomorphogenesis: lighting up their shape”. In: *International Journal of Astrobiology* 22.1 (Feb. 2023), pp. 33–56. ISSN: 1473-5504. DOI: 10.1017/S1473550422000313.

[23] J. Johnson and J. P. Grotzinger. “Affect of Sedimentation on Stromatolite Reef Growth and Morphology, Ediacaran Omkyk Member (Nama Group), Namibia”. In: *South African Journal of Geology* 109.1-2 (June 2006), pp. 87–96. ISSN: 1012-0750. DOI: 10.2113/gssajg.109.1-2.87.

[24] A. Curtis et al. “Modelling Ediacaran metazoan–microbial reef growth”. In: *Sedimentology* 68.5 (Aug. 2021), pp. 1877–1892. ISSN: 0037-0746. DOI: 10.1111/sed.12832.

[25] P. Szymczak et al. “Shapes of ideal stalagmites”. In: *Proceedings of the National Academy of Sciences of the United States of America* 122.42 (2025). ISSN: 10916490. DOI: 10.1073/pnas.2513263122.

[26] B. Chopard, H. J. Herrmann, and T. Vicsek. “Structure and growth mechanism of mineral dendrites”. In: *Nature* 353.6343 (1991). ISSN: 00280836. DOI: 10.1038/353409a0.

[27] Z. Hou et al. “Mineral dendrites: Indicators for geological aqueous environments”. In: *Earth-Science Reviews* 270 (2025). ISSN: 00128252. DOI: 10.1016/j.earscirev.2025.105231.

[28] Z. Hou et al. “Three-dimensional mineral dendrites reveal a nonclassical crystallization pathway”. In: *Geology* 51.7 (2023). ISSN: 19432682. DOI: 10.1130/G51127.1.

[29] G. Datseris, A. R. Vahdati, and T. C. DuBois. “Agents.jl: a performant and feature-full agent-based modeling software of minimal code complexity”. In: *SIMULATION* 100.10 (Oct. 2024), pp. 1019–1031. ISSN: 0037-5497. DOI: 10.1177/00375497211068820.

[30] K. Hickman-Lewis et al. “Advanced two- and three-dimensional insights into Earth’s oldest stromatolites (ca. 3.5 Ga): Prospects for the search for life on Mars”. In: *Geology* 51.1 (Jan. 2023), pp. 33–38. ISSN: 0091-7613. DOI: 10.1130/G50390.1.

[31] T. A. Witten and L. M. Sander. “Diffusion-limited aggregation, a kinetic critical phenomenon”. In: *Physical Review Letters* 47.19 (1981). ISSN: 00319007. DOI: 10.1103/PhysRevLett.47.1400.

[32] V. A. Petryshyn et al. “Stromatolite lamination frequency, Walker Lake, Nevada: implications for stromatolites as biosignatures”. In: *Geology* 40.6 (2012), pp. 499–502. DOI: 10.1130/G32675.1.

[33] J. Szulc and B. Smyk. “Bacterially controlled calcification of freshwater Schizothrix-stromatolites: an example from the Pieniny Mts, Southern Poland”. In: *Phanerozoic Stromatolites II*. Springer, 1994, pp. 31–51. DOI: 10.1007/978-94-011-1124-9_2.

[34] S. McMahon and J. Cosmidis. “False biosignatures on Mars: anticipating ambiguity”. In: *Journal of the Geological Society* 179.2 (2022). ISSN: 00167649. DOI: 10.1144/jgs2021-050.

[35] N. McLoughlin, L. A. Wilson, and M. D. Brasier. “Growth of synthetic stromatolites and wrinkle structures in the absence of microbes – implications for the early fossil record”. In: *Geobiology* 6.2 (Mar. 2008), pp. 95–105. ISSN: 1472-4677. DOI: 10.1111/j.1472-4669.2007.00141.x.

[36] J. Gong et al. “Morphogenesis of digitate structures in hot spring silica sinters of the El Tatio geothermal field, Chile”. In: *Geobiology* 20.1 (2022). ISSN: 14724669. DOI: 10.1111/gbi.12471.

Supplementary Information

In this supplementary information, we give detailed descriptions of all parameters, list the parameters used, and describe the quantitative measurements made. Furthermore, we give more details on the running of the interactive model, the model implementation, and model extensibility.

Contents

A Tutorial on the Interactive Simulation

Interactive simulations require installation of the `Julia` programming language and the relevant packages; however, when this is installed, it should be possible to run with minimal interface with the actual code. `Julia` language can be installed, with little effort, following the detailed documentation of the language provider `https://julialang.org/`.

We provide two ways to launch the interactive interface. One is using a Jupyter Notebook which a user can run or by running the executable `.jl` file directly. In both cases, the relevant packages, `[Agents, LinearAlgebra, Random, StatsBase, GLMakie]`, must be installed. The `.jl` file is configured so that the relevant packages are automatically checked for and installed. This means that the interactive simulation can simply be launched by typing `julia -i "path to .jl file"` into your system terminal or command prompt and the interactive simulation will begin. The sleep function should be set to zero if you do not want pauses between time steps, and the number of steps per frame can be set by changing the `dt` parameter. The simulation will begin with default settings, where the initial conditions and range of variables on the sliders are something that can be changed by updating the code. The interactive code file is minimal, so all relevant variables can be found at the end of the file. Additional details can be found in the code repository.

A.1 Video of Simulation Runs

Similarly to the interactive interface, there is a way to directly generate videos from the `Agents.jl` simulations. In the supplementary material, we attach a few videos where runs can be visualised and attach a notebook which can be used to generate these videos. We select 15 time steps per frame to decrease the file size. Full parameter lists are given in the parameters section.

B Parameter Descriptions

In this section, we describe each of the parameters used in this work in more detail. The model contains the following parameters, broken into three categories.

B.1 Agent Properties

- Precipitation Amplitude - Maximum probability for a precipitating agent to add precipitate to a neighbouring cell and spread. This value multiplies any periodic function. This controls much of the final morphology and the observed layers. This parameter aims to approximate the aggregate physics, chemistry, and biology that control the rate of microbial induced precipitation, such as the pH, available carbonate, temperature, and microbial activity.
- Removal Probability - Probability for the precipitating agent to be removed at each step. This represents a local disruption of the microbial mat or fluctuations that prevent precipitation at a location.
- Precipitation Weights - Vector of length 3 which sets the relative preferences for upward, horizontal, or downward precipitation. This approximates the hypothesis that microbial activity may tend to push growth upwards for photosynthesis. However, this may not be the case in all scenarios, so this can be modified.

- Stability Distance - Stability distance for sediment agents. This is a parameter derived from the DLA that represents the ability of the sediment to settle and fall to a stable position. This would depend on the environmental conditions and the adhesion of the mat driven by EPS.
- Attraction Distance - Attraction distance for sedimenting agents. This is a parameter inspired by DLA that drives the morphology. This represents the distance at which the sediment agents stick to the structure. This is related to the adhesive properties of the microbial mat and the environmental conditions.
- Recolonisation Probability - Probability of introducing a precipitate agent where the sediment lands. This is the probability that microbial activity covers newly arrived sediment.
- Down speed - Fixed size of vertical random walk steps. This down speed represents the step size of the biased random walks of the particles downwards. If this number is large, it would represent ballistic motion, which can prevent the formation of some morphologies.
- Side speed - Fixed size of horizontal random walk steps. This parameter controls how fast the particles move side to side when doing the random walk. We can also bias this if necessary to represent a flow.
- Conical Scaling - The parameter that governs how much the growth rate is rescaled depending on the number of solid neighbours above the agent. This can be set to zero to disable this behaviour, with positive values leading to more tip dominated growth.
- Prevent Overhangs - This boolean value sets the kind of overhanging which are allowed by the model. This can prevent mushroom shapes with a flat overhang or allow them.

B.2 External Forcing

- Sediment Amplitude - The maximum amount of sediment agents added at each step. This causes the structure to grow by sedimentation and must be a whole number. A rescaled version of this could also be constructed, which varies depending on the simulation grid width to maintain the sediment density.
- Period Control Parameter - Scaling of oscillations for given periodic functions that affect the sediment and precipitation. Mathematical definition in the main text. This potentially represents a variety of environmental periodic behaviours or timescales.
- Precipitate Agent Period Scaling - Multiplicative constant that sets how much the precipitate cycles scale to the sediment cycles. See the main text for mathematical details.
- Precipitate Agent Period Offset - Offsets the cycles of the precipitate agents by a given constant. See the main text for mathematical details.
- Sediment Forcing Function - This is the choice of function to set the oscillations. This must be positive, so we give the following options: $\max(\cos x, 0)$, $\cos^2 x$, or $|\cos x|$.
- Precipitation Forcing Function - This is the choice of function to set the oscillations. This must be positive, so we give the following options: $\max(\cos x, 0)$, $\cos^2 x$, or $|\cos x|$.

B.3 Model Setup Parameters:

- Initial Conditions - Choice of whether to set a flat layer, patches, triangular, a mound, or sinusoidal initial substrate.
- Model Width - Width of the simulation grid. The grid is horizontally periodic. A key detail is that the sediment amplitude and grid width will interplay as this affects the density of sediment per cell.
- Model Height - Height of the simulation grid. This sets how long the simulation can run before the solid fills the grid and the number of layers visible.
- Distance Metric - Can be set in Agents.jl, we choose to use Euclidean, for this work, but may also use Manhattan if preferred.
- Initial Precipitate Agent Density - The density of initial precipitate agents placed on the available substrate.

C Conical Structure and Model Extensibility

One key morphology of stromatolites is conical forms. They have been well modelled, as in the work of [21], and are similar in gross morphology to abiotic objects such as stalagmites [25]. In this work, we do not reproduce the specific physics of models such as those applied in Petroff et al. [21] and Szymczak et al. [25]. However, we show how our model which does not natively produce conical morphologies can be relatively easily modified to create heuristic-conical like structures. This allows us to have a minimal model of cone formation coupled to our model of internal microbialite structure.

Conical structures, be they biotic or abiotic without overhangs, are generally formed when the apex of the structure grows faster than the surrounding areas, producing a leading point which grows ahead of the rest of the structure. This may be as a result of diffusion-driven processes [21] or shadowing, depending on whether such mechanisms are considered applicable to the object in question.

The heuristic we add to the model is as follows: When assessing the likelihood for microbial induced precipitation, we rescale it by an exposure factor. We do this by multiplying the precipitation probability by this factor, which is defined as $(1 + n_{\text{above}})^{-c}$ where c is the conical scale parameter, which must be non-negative and n_{above} is the number of neighbours above. This is largest when the agent has no neighbours in the row of cells above, at a tip, but reduced when the agent has any neighbour blocking it. When c is zero, we see no effect and higher values of c make the cone more peaked. Additionally, we modify the preferred growth direction to have a stronger preference for upward growth. These changes allow various conical type structures to be found with precise morphology depending on the interplay of all parameters. To maintain physical plausibility and prevent unrealistic overhangs (e.g., mushroom-shaped structures), we also enable a flag which can be turned on to prevent horizontal overhangs by only allowing growth if there is supporting structure directly or diagonally below.

Conical structures are initial conditions dependent, as these shape how the central tip emerges. In order to create centred conical structures, we start the cones growing from small triangles to allow the tip to grow at the intended location. This also prevents impassable walls from forming at

the edge of the initial conditions due to overhangs at $t = 0$. The shape of the cone is sensitive to the curvature of the initial structure, as the growing layers are influenced by the previous layer, with this influence extending back to the initial shape to various degrees, depending on the parameter combination.

To maintain the growth of conical structures, we require a very low or zero microbial agent removal probability and a recolonisation probability close to one, as if the one pixel which is growing at the local tip is removed; this can have a negative effect on the emergence of the conical structure. Our cones may display fractal-like behaviour, where a large cone forms with a surface made of smaller conical features.

In our model, conical stromatolites occur in the mineral precipitation dominated regime, where the conical form is the result of the preferred direction of precipitation and not directly caused by the actions of sediment. Depending on the interplay between the parameters, layers may or may not appear in the conical structures. One challenge in making even small additions to a model like this is the potential cascade of effects from the changes. In this case, modifying the precipitation probability by the exposure factor reduces this key control parameter, which then changes the range in which other changes in morphology occur. Hence, we do not dwell on the specific of the conical-like structures, but show how our model can be modified to capture various effects and parsimoniously reproduced key structures.

An example of a heuristic-conical morphospace is given in figure 7, (detailed parameters given in table 7). The extent to which these structures appear conical depends on both the conical scale parameter and the precipitation amplitude as shown. However, as the model lacks settling dynamics where the structure relaxes, we do not make true triangular cones but end up with cones that are more vertical and pine-cone-shaped. This demonstrates how the model can be updated in some cases quite easily, but other changes would require a more fundamental rewriting of the logic.

D Quantitative Analysis of Structure

In previous related work on modelling of stromatolites [17], most of the work has been qualitative. However, we propose linking the input parameters with variables that can describe the output structures. This allows an indication of where in parameter space changes in morphology occur and which parameters control various aspects of the structure.

D.1 Measurements Made

We aim to measure a reasonable range of properties which are computationally efficient and summarise the morphology of the objects. Thus we aim to select quantities which minimise intra measurement correlation aside from the case of obvious parameters like the mean and maximum height, for example. The selected set of measurements assumes that we are starting from flat initial conditions and that we have uniform horizontal behaviour throughout the model for simplicity. If you implemented localised initial conditions or other parameters which break the uniformity of the structures, then modified measurements would need to be used to account for this. A full list and description of the eleven measured quantities is given in section G .

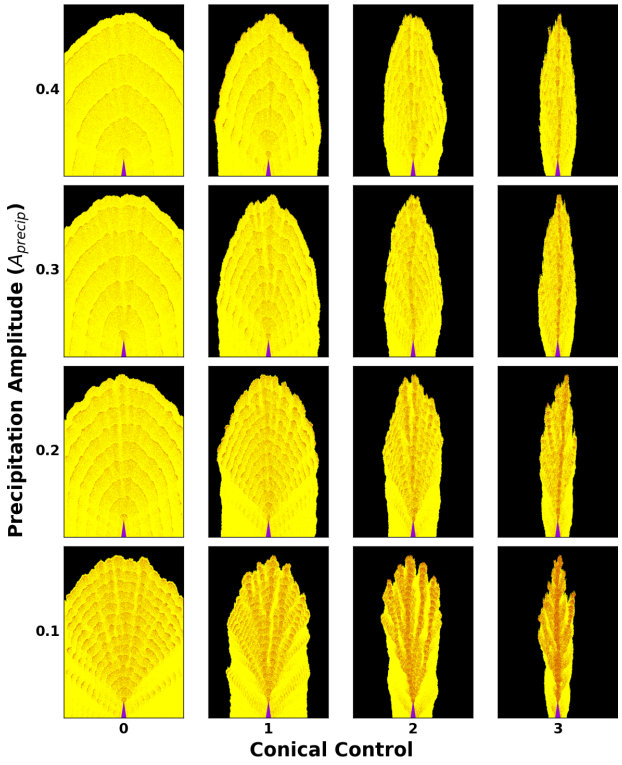

Figure 7. Modified simulation in attempt to make conical-like stromatolites. Increasing the conical scale parameter leads to more preference for vertical growth while spreading and internal morphology are modified by the precipitation amplitude. Precipitation in yellow, sediment in red.

D.2 Parameter Values Tested

When quantitatively studying morphology we use two parameter sweeps focusing on precipitation amplitude, stability distance, and attraction distance. We do one sweep with varying precipitation amplitude and one with this parameter fixed. This allows us to see in more detail the impact of the structural parameters as the precipitation rate can obscure other trends as it has a strong control of morphology and can overwhelm the other parameters. All other parameters are fixed for this parameter sweep, to the values given in appendix, F.3.

In order, to sample the parameter space and to have control over the number of samples while fixing the parameter range we use Latin Hypercube sampling to generate 1500 samples doing 10000 time steps per sample. Latin hypercube sampling generates random samples such that the space is partitioned by the samples and samples are approximately evenly distributed across the space. Each simulation is an independent process, so we can run this in parallel using `Julia` multi-threading and generate large numbers of samples efficiently on a laptop. We generate the same number of samples for each sweep using Latin Hypercube sampling irrespective of the dimensionality of the sampling space, with the sampling plan floored to integers for parameters which require this.

Due to the large number of measurements made, there are a large number of combinations of measurements and parameters that could be plotted. In the text, we give a small selection of these

and in the supplementary material attach all the pairwise combinations of parameter plots, the raw data and `.jpg` image for each simulation, and a `.csv` of all values across simulations.

D.2.1 Sweep 1

In the first sweep, we sweep the stability and attraction distance in the set $[1, 50]$ and vary the precipitation amplitude parameter between $[0.01, 0.3]$. Increasing the precipitation amplitudes to larger values outwith this range tends to result in morphologies where most of the grid is filled with mainly precipitate.

D.2.2 Sweep 2

In the second sweep, we wish to isolate the effects of stability and attraction distances, so we set the range for each as integers in the set $[1, 50]$ and fix the precipitation parameters.

D.3 Quantitative Analysis - Parameter Sweep 1

The results of the first parameter sweep are given in figure 8, which shows how precipitation rate controls various aspects of the morphologies. Figure 8a, shows the relationship between the fraction of the solid object made up of precipitate and the input precipitation amplitude. As expected, there is a strong correlation, with an almost linear trend, between the input precipitation amplitude and the observed precipitate, showing that the model intuitively behaves as expected.

The effect on precipitation amplitude on the structure can be quantified by using the gzip compression ratio, which measures the file size of the uncompressed object to the file size of the compressed object using the gzip algorithm. gzip compressibility is a very simple way (although with caveats) to asses the complexity. It gives a sense of how easy the object is to compress, features a uniform structure or repeating patterns, or how far it is from random noise, more difficult to compress. Figure 8b shows that as we increase the precipitation amplitude, we decrease the compressibility because we create more mixing of precipitate and sediment making it harder for the algorithm to compress. In the low-precipitation regime, there is still a large variation in compressibility, as the different morphologies all compress to varying degrees due to their intrinsic complexity.

The dependence of the maximum height of the generated object on the stability distance and the precipitation amplitude is given in figure 8c. The maximum height tends to increase as you increase precipitation as more solid structure is formed. However, the tallest structures occur when the stability distance is low and the sediment particles cannot rearrange, sticking directly to the tallest branches driving the structure upward.

The interplay between precipitation amplitude and attraction distance on roughness (measured as the coefficient of variation of the object height per column) is given by figure 8d. This shows how high attraction distances promote branching, leading to higher measured roughness but that this can be suppressed by high precipitation rates, which fill in the gaps between branches. This reveals how certain aspects of the morphology can be suppressed by high precipitation regimes.

D.4 Quantitative Analysis - Parameter Sweep 2

In this parameter sweep, figure 9, we more clearly expose the interactions between stability and attraction distance in the formation of the morphology by fixing the precipitation amplitude.

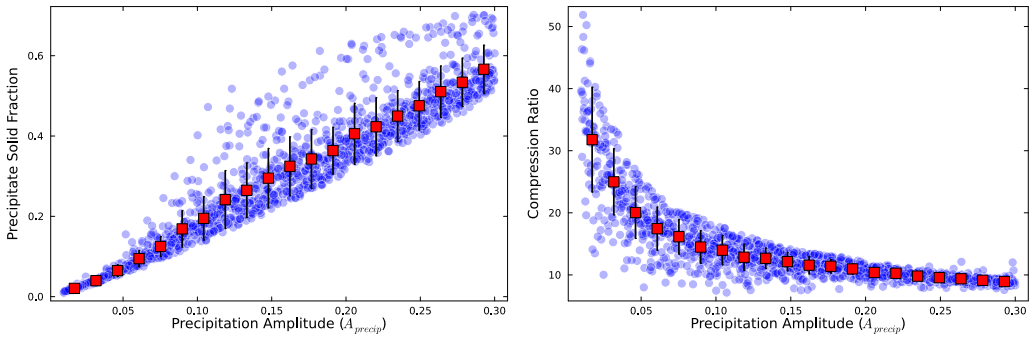

(**a**) Increasing precipitation amplitude leads to higher fraction of precipitate as expected

(**b**) Variations in measured structural complexity with precipitation amplitude

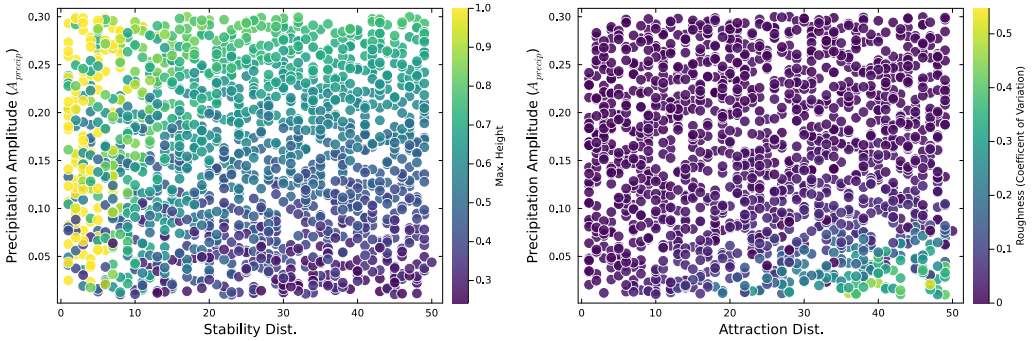

(**c**) Interplay between stability distance and precipitation amplitude on maximum height

(**d**) Variation in roughness (measured by coefficient of variation) with precipitation amplitude and attraction distance

Figure 8. Subset of quantitive structural trends caused by parameter variation in parameter sweep one. Each point is a unique simulation. Red squares are the mean values of local binned region, with error bars one standard deviation within these bins.

Figure 9a, shows how roughness (measured by the coefficient of variation of the surface) correlates with the attraction distance due to the tendency for larger attraction distances to lead to branching, where the stability distance allows. This matches the trends observed when viewing the qualitative morphospaces of stability and attraction distance.

Similar trends can be captured by figure 9b, which shows how the mean filled fraction in each row of the object varies with stability distance. The mean filled fraction approaches one when all the rows are filled and we have a uniform solid structure while it is smaller when we have a columnar or branching structure that has gaps. For larger stability distances, the number of columns decreases until the sediment settles across the domain uniformly, whereas smaller stability distances lead to a variety of filled fractions depending on the density of the branching caused by the attraction distance.

In agreement with the qualitative impression given by the morphospaces, the variation in compressibility highlights the array of morphologies that result from varying the stability and attraction distance as different regions of the plot show distinct behaviour, figure 9c. For low

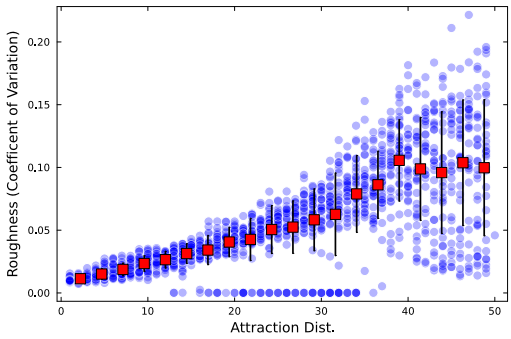

(**a**) Increasing in branching caused by increase in attraction distance observed increase in roughness (measured by coefficient of variation)

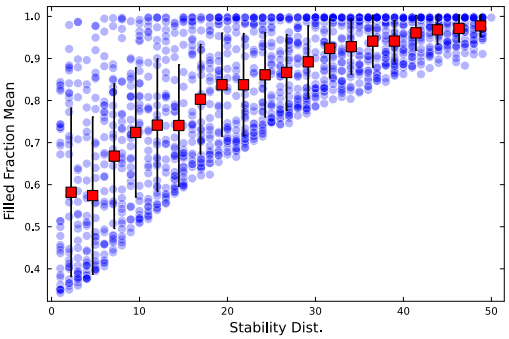

(**b**) Increasing stability distance leading to increase in mean filled fraction (horizontally across rows)

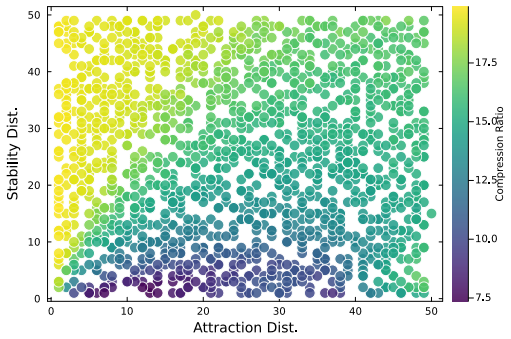

(**c**) Interplay of stability and attraction distances on complexity as measured by the compressibility

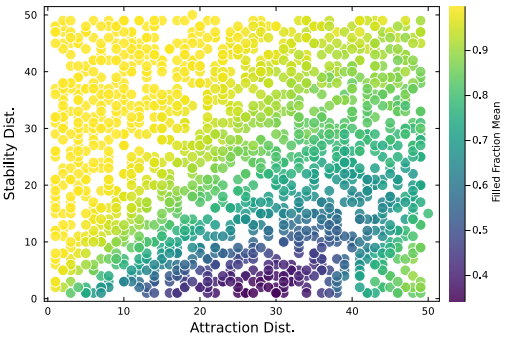

(**d**) Mean filled fraction with stability distance and attraction distance showing distinct types of morphologies created.

Figure 9. Subset of quantitive structural trends caused by parameter variation in parameter sweep two. Each point is a unique simulation. Red squares are the mean values of local binned region, with error bars one standard deviation within these bins.

attraction distance and intermediate to high stability distance, we see higher compressibility due to the regular planar structures formed. For higher attraction distances with low stability distances, we see reduced compressibility from the emergence of branching structure. With more intermediate compressibility due to columnar structures when both distances are larger. Eventually, very large attraction distances also lead to column-like structures as sediment sticks to the side of the growing branch and not just the tip region.

Similar regional trends can be observed when plotting the mean filled fraction against both stability and attraction distances, figure 9d. The same variation as in figure 9c where different parameter combinations lead to branching, columns, and flat layers, which are captured by this distinct measurement.

D.5 Correlation between Input Parameters and Measurements

The observed morphologies are not necessarily easily described by a few measurements, and various measurements can be used to describe different aspects of the morphology. These may correlate with each other and the input parameters in many ways. In figure 10, we plot the correlation between the input parameters and the measured quantities for both parameter sweeps to provide a concise way to summarise the interactions.

The differences in correlation between figures 10a and 10b highlight the impact that the choice of parameters to sweep can have on the observed correlation. Similar trends to previously observed can be picked out of the correlation matrices. The stability distance controls the transition between flat layers and columns. The attraction distance controls the emergence of branching. Increasing precipitation leads to thicker layers and smooths out the structure. The correlation matrices also show the correlation between measurements, showing how different measurements can capture similar aspects of the structure.

E Additional Model Details

E.1 Initial Conditions Setup

The morphologies which emerge from the simulations are highly initial conditions dependent. Due to the flexible framework, initial conditions can be implemented with a wide variety of structures. In this work, we use several examples. The simplest is to simply set all cells at the base of the grid to the value 1, representing a solid substrate. Another option we use is localised initial conditions where the 10 cells at the centre of the base of the grid are set to solid and the rest are left empty. We also give the option for a few more complex shapes. Firstly, in order to make the structure more conical, we allow triangular initial conditions where we generate a solid triangle at the centre of the grid 100 cells tall and 30 cells wide at the base. We also allow the user to generate a small mound at the centre of the bottom of the grid, of height 10 and width 150 where the height decays quadratically. The most complex initial condition we implement is a sinusoidal function to simulate roughness. This function fills in all the cells below an integer generated by rounding $5\sin(\frac{2\pi x}{300}) + |\eta|$ where x is the distance across the base and η is a normally distributed random variable generated using the `randn()` function. Initial conditions can be modified as the user desires, and we do not focus on the more complex initial conditions as they are not used in this work. For example, in future work it is possible that the roughness function would be modified to make the behaviour more realistic, and the noise stronger.

E.2 Morphospace Setup

The code automatically places figures in the morphospace in such a way that it should fit if you vary the size and number of figures. However, to make the output easier to read in the main text we manually alter the spacing between plots and the background colours of the canvas on which the plots are placed. All actual simulation morphospace plots are directly output by the code.

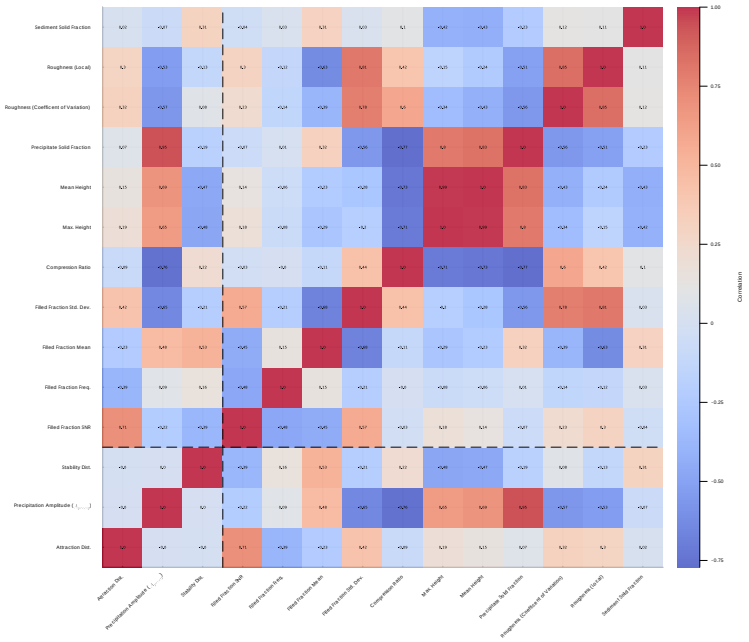

(**a**) Correlation matrix derived from varying precipitation amplitude, stability distance and attraction distance. All other parameters fixed.

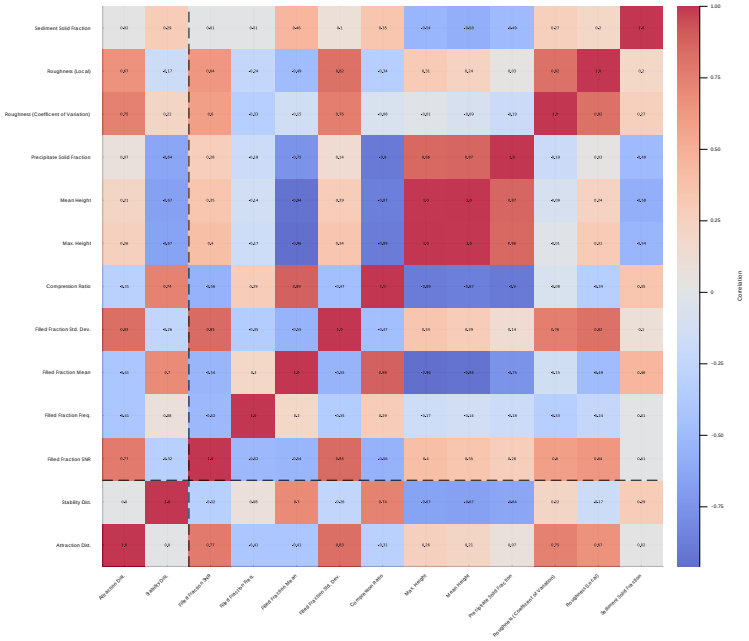

(**b**) Correlation matrix derived from varying stability distance and attraction distance. All other parameters fixed.

Figure 10. Correlation matrices when fixing and sampling different regions of parameter space. Varying precipitation growth rate suppressing trends visible in the stability and attraction distance only correlation matrix. Correlation values represent the Pearson correlation coefficient.

F Parameter Values Set

In this section, we describe the set of parameters which we use in various scenarios. For ease of use, the code assumes a set of default parameters, and then a user only needs to input the parameters when they deviate from the default values. In this document, we list the default parameters and then highlight when we use values which deviate from the defaults given in table 1. The default parameter are not special or optimal values and should be thought of as arbitrarily selected within the range which should lead to functional results.

Table 1. Default Parameters Used in the Simulation

Parameter	Type	Default	Description
`width`	`Int`	1000	Width of the domain.
`height`	`Int`	400	Height of the domain.
`initial_solid_setup_type`	`Symbol`	`:base_line`	Initial condition type (`:rough`, `:mound`, `:triangle` or `:base_line`).
`downspeed`	`Int`	3	Vertical step speed for particles.
`sidespeed`	`Int`	1	Horizontal step speed for particles.
`precip_amplitude`	`Float64`	0.08	Maximum Probability of Precipitation, coefficient of precipitation periodicity function
`remove_probs`	`Float64`	0.02	Probability of precipitating agent removal per time step.
`precip_weights`	`Vector`	[0, 1, 1]	Growth direction preferences (down, side, up).
`sediment_amplitude`	`Int`	50	Maximum value for the sedimentation rate, coefficient of sediment periodicity function.
`period_control_T`	`Float64`	200	Sets length of oscillations for given periodic functions (proportional to period, exact realtionship depends on function choice)
`precip_period_scaling`	`Float64`	1	Relative scaling of precipitation vs. sedimentation period.
`precip_period_offset`	`Float64`	50	Phase offset for precipitation oscillations.
`stability_dist`	`Int`	15	Stability distance for the DLA process.
`attraction_dist`	`Int`	15	Attraction distance for the DLA process.
`conical_scale`	`Float64`	0	Bias for tip-growth (conical structures), set to zero for no bias.
`distance_metric`	`Symbol`	`:euclidean`	Metric used for distances (`:euclidean`, `:manhattan`, `:chebyshev`[may give non-physical behaviour]).
`initial_microbe_density`	`Float64`	0.9	Initial substrate precipitating agent proportion.
`recolonisation_prob`	`Float64`	0.5	Likelihood of precipitating agents appearing on new sediment.
`sediment_periodic_mode`	`Symbol`	`:abs`	Periodic function behaviour for sediment. Options `:abs`,`:max_cos`, `:cos2`, `:constant`
`precip_periodic_mode`	`Symbol`	`:abs`	Periodic function behaviour for microbes. Options `:abs`,`:max_cos`, `:cos2`, `:constant`
`prevent_overhang`	`Bool`	`false`	Flag to restrict horizontal overhangs.

In the following subsections, we list all the deviations from the default parameters used to generate the figures in the main text.

F.1 Comparison to Real Objects Parameters

In this section, we list the non-default parameters which were set in order to match the qualitative features of several categories of real microbialites presented in the main text. The parameters used give the desired structure; however, in general there are likely many more parameter sets that could give similar structures, which we do not fully and exhaustively explore. Additional combinations can be tested using the interactive framework.

The Goose Egg Formation structure with flat laminations relies on small stability and attraction distances, and uses the parameters given in table 2.

Table 2. Non-Default Parameters used to reproduce Goose Egg Formation flat laminations

Parameter	Value
`width`	2000
`height`	1900
`precip_amplitude`	0.05
`precip_weights`	[1,1,10]
`sediment_amplitude`	100
`period_control_T`	2000
`stability_dist`	3
`attraction_dist`	1
`recolonisation_prob`	0.99
`sediment_periodic_mode`	`:max_cos`
`precip_periodic_mode`	`:max_cos`

Domal morphologies can be formed in a similar vein to planar laminations aside from using localised initial conditions, slightly more precipitation, and more even growth axis. table 3.

More irregular layers which tend towards columnar structures can be formed by increasing the stability and attraction distances reproducing the qualitative structure of the linked-columnar stromatolite from the El Molino Formation, table 4.

Finally, branching can be formed by imposing a higher attraction distance with a low stability distance. In addition to using localised initial conditions, this allows us to reproduce the branched domal microbialite of the Howe Limestone Member listed in the main text, table 5.

F.2 Morphospace Parameters

When creating the morphospace plots we leave all parameters as default aside from those directly written on the figures and the ones mentioned in the table 6 for the non-conical morphospaces and table 7 for the conical morphospaces.

F.3 Quantitative Sweep Parameters

When performing the quantitative parameter sweep we fix the following non-default values, table 8, and sweep over the parameters in the range and density described in the quantitative analysis

Table 3. Non-Default Parameters used to reproduce Campbellrand-Malmani Subgroup Stromatolite

Parameter	Value
`width`	2000
`height`	1900
`initial_solid_setup_type`	`:localised`
`precip_amplitude`	0.1
`precip_weights`	[1,1,3]
`sediment_amplitude`	100
`period_control_T`	2000
`stability_dist`	3
`attraction_dist`	1
`recolonisation_prob`	0.99
`sediment_periodic_mode`	`:max_cos`
`precip_periodic_mode`	`:max_cos`

Table 4. Non-Default Parameters used to reproduce linked-columnar stromatolite

Parameter	Value
`width`	2000
`height`	1950
`precip_amplitude`	0.08
`precip_weights`	[1,1,3]
`sediment_amplitude`	100
`period_control_T`	2000
`stability_dist`	35
`attraction_dist`	20
`recolonisation_prob`	0.99
`sediment_periodic_mode`	`:max_cos`
`precip_periodic_mode`	`:max_cos`

Table 5. Non-Default Parameters used to make Branched Domal Microbialite from the Howe Limestone Member formation

Parameter	Value
`width`	2000
`height`	1900
`initial_solid_setup_type`	`:localised`
`precip_amplitude`	0.1
`precip_weights`	[1,1,3]
`sediment_amplitude`	100
`period_control_T`	2000
`stability_dist`	5
`attraction_dist`	20
`recolonisation_prob`	0.99
`sediment_periodic_mode`	`:max_cos`
`precip_periodic_mode`	`:max_cos`

Table 6. Non-Default Parameters Used in the Non-Conical Morphospace

Parameter	Value
`width`	700
`height`	1000
`precip_weights`	[1,1,3]
`period_control_T`	1000
`recolonisation_prob`	0.99
`sediment_periodic_mode`	`:max_cos`
`precip_periodic_mode`	`:max_cos`

Table 7. Non-Default Fixed Parameters Used in the Conical Morphospace

Parameter	Value
`width`	700
`height`	1000
`initial_solid_setup_type`	`:triangle`
`remove_probs`	0
`precip_weights`	[0,1,10]
`sediment_amplitude`	25
`period_control_T`	1000
`conical_scale`	2
`recolonisation_prob`	0.99
`sediment_periodic_mode`	`:max_cos`
`precip_periodic_mode`	`:max_cos`
`prevent_overhang`	`true`

section in the main text. In the main text, we show a few examples of generated single stromatolites when discussing equifinality. For the first sweep, we use *sim_20260317_143341_f10c02e5* which has roughness value 0.0080, stability distance 43, attraction distance 6 and precipitation amplitude 0.2938 compared to which has *sim_20260317_143302_a96b6ea8* roughness value 0.0115, stability distance 46, attraction distance 47 and precipitation amplitude 0.2942. Which have a broadly similar structure for very different parameters. While for the second sweep, we use *sim_20260317_144700_c365419c* mean filled fraction 0.9886, stability distance 35, and attraction distance 18 compared to *sim_20260317_144627_6f24fc37* mean filled fraction 0.9976, stability distance 48, and attraction distance 1. These examples have quite different parameters and structures but similar mean filled fraction.

Table 8. Non-Default Parameters Used in The Quantitative Parameter Sweeps

Parameter	Value
`width`	700
`height`	1500
`sediment_amplitude`	70
`period_control_T`	1000
`sediment_periodic_mode`	`:max_cos`
`precip_periodic_mode`	`:max_cos`

F.4 Video Parameters

We generate a few videos to highlight the dynamics. For each video, we keep all the non-default parameters the same and pick pairs of stability and attraction distances. The non-default parameters are given by table 9.

The stability and attraction distances are given in the following manner: [video 1, video 2, video

Table 9. Non-default Video Parameters (does not include stability and attraction distance values, see text)

Parameter	Value
`width`	2000
`height`	1900
`precip_amplitude`	0.1
`precip_weights`	[1,1,3]
`sediment_amplitude`	100
`period_control_T`	2000
`recolonisation_prob`	0.99
`sediment_periodic_mode`	`:max_cos`
`precip_periodic_mode`	`:max_cos`

3] = [[30,30], [5,30], [30,2]] where the order is given by [stability distance, attraction distance]. Videos are run for 2000 frames at 15 steps per frame.

G Quantities Measured

In order to quantitatively capture the emergent structures, we devise a range of simple measurements which capture various aspects of the morphology.

We measure the following parameters:

1. Sediment Fraction - Fraction of cells of the total grid filled by sediment.
2. Precipitate Fraction - Fraction of cells of the total grid filled by precipitate.
3. Scaled maximum height - Maximum height of the structure scaled by the grid height
4. Scaled mean height - Mean height of the structure per column scaled by the grid height
5. Roughness (Coefficient of Variation) - Standard Deviation of the column heights divided by the mean column heights.
6. Roughness (local) - Root Mean Square (RMS) of the local height differences between columns.
7. Mean Filled Fraction (column wise) - Mean proportion of filled cells in each column up to the maximum highest filled cell in that column
8. Standard Deviation of Filled Fraction (column-wise) - Standard Deviation of proportion of filled cells in each column up to the maximum highest filled cell in that column
9. FFT derived frequency of Filled Fraction (column wise) - Frequency of oscillation in filled fraction derived from FFT
10. FFT derived signal-to-noise-ratio of Filled Fraction (column wise) - Signal-to-noise-ratio of FFT peak derived from filled fraction

11. Gzip Compression ratio - The ratio of the uncompressed sized divided by the compressed size, larger means more compression and regularity using gzip by calling `transcode(GzipCompressor, ...)` inside `Julia`.

This list of measurements is simply a subset of potential measurements as there are many ways to describe a complex structure such as microbialites. These parameters are selected based on the fact that they are computationally efficient, reasonably easy to interpret and fulfil the needs of this work. Quantification of bespoke morphologies in more detail may require a more bespoke measurement set.

References

[1] R. V. Burne and L. S. Moore. "Microbialites: organosedimentary deposits of benthic microbial communities". In: *Palaios* (1987), pp. 241–254. DOI: 10.2307/3514674.

[2] R. E. Riding and S. M. Awramik. *Microbial sediments*. Springer Berlin, Heidelberg, 2000. DOI: 10.1007/978-3-662-04036-2.

[3] K. Grey and S. M. Awramik. "Handbook for the study and description of microbialites". In: *Geological Survey of Western Australia Bulletin* 147 (2020).

[4] M. J. Van Kranendonk et al. "Geological setting of Earth's oldest fossils in the ca. 3.5 Ga Dresser formation, Pilbara Craton, Western Australia". In: *Precambrian Research* 167.1-2 (2008), pp. 93–124. DOI: 10.1016/j.precamres.2008.07.003.

[5] K. Hickman-Lewis et al. "Most ancient evidence for life in the Barberton greenstone belt: Microbial mats and biofabrics of the 3.47 Ga Middle Marker horizon". In: *Precambrian Research* 312 (2018), pp. 45–67. DOI: 10.1016/j.precamres.2018.04.007.

[6] L. Fogret, P. Sansjofre, and S. V. Lalonde. "Geochemistry of carbonate microbialites through time and space: Insights from the microbialite collection of the Muséum National d'Histoire Naturelle (MNHN), France". In: *Chemical Geology* 662 (2024), p. 122239. DOI: 10.1016/j.chemgeo.2024.122239.

[7] R. P. Reid et al. "Microbialite accretion and growth: lessons from Shark Bay and the Bahamas". In: *Annual review of marine science* 16.1 (2024), pp. 487–511. DOI: 10.1146/annurev-marine-021423-124637.

[8] J. M. García Ruiz et al. "Morphology: an ambiguous indicator of biogenicity". In: *Astrobiology* 2.3 (2002), pp. 353–369. DOI: 10.1089/153110702762027925.

[9] M. J. Van Kranendonk et al. "A review of 3.7 Ga stromatolites from the Isua Supracrustal Belt, West Greenland". In: *Earth-Science Reviews* 262 (2025), p. 105034. DOI: 10.1016/j.earscirev.2024.105034.

[10] A. P. Nutman et al. "Rapid emergence of life shown by discovery of 3,700-million-year-old microbial structures". In: *Nature* 537.7621 (2016). ISSN: 14764687. DOI: 10.1038/nature19355.

[11] S. W. Ruff and J. D. Farmer. "Silica deposits on Mars with features resembling hot spring biosignatures at El Tatio in Chile". In: *Nature Communications* 7 (2016). ISSN: 20411723. DOI: 10.1038/ncomms13554.

[12] C. Dupraz et al. "Stromatolitic knobs in Storr's Lake (San Salvador, Bahamas): A model system for formation and alteration of laminae". In: *Geobiology* 11.6 (2013). ISSN: 14724677. DOI: 10.1111/gbi.12063.

[13] M. T. Batchelor et al. "Deterministic KPZ model for stromatolite laminae". In: *Physica A: Statistical Mechanics and its Applications* 282.1 (2000). ISSN: 03784371. DOI: 10.1016/S0378-4371(00)00077-7.

[14] M. Batchelor et al. "A case for biotic morphogenesis of coniform stromatolites". In: *Physica A: Statistical Mechanics and its Applications* 337.1-2 (June 2004), pp. 319–326. ISSN: 03784371. DOI: 10.1016/j.physa.2004.01.065.

[15] M. Batchelor et al. "Statistical physics and stromatolite growth: new perspectives on an ancient dilemma". In: *Physica A: Statistical Mechanics and its Applications* 350.1 (May 2005), pp. 6–11. ISSN: 03784371. DOI: 10.1016/j.physa.2005.01.014.

[16] R. Cuerno et al. "Pattern formation in stromatolites: Insights from mathematical modelling". In: *Journal of the Royal Society Interface* 9.70 (May 2012), pp. 1051–1062. ISSN: 17425662. DOI: 10.1098/rsif.2011.0516.

[17] C. Dupraz, R. Pattisina, and E. Verrecchia. "Translation of energy into morphology: Simulation of stromatolite morphospace using a stochastic model". In: *Sedimentary Geology* 185.3-4 (Mar. 2006), pp. 185–203. ISSN: 00370738. DOI: 10.1016/j.sedgeo.2005.12.012.

[18] H. J. Hofmann. "Attributes of Stromatolites". In: *Geological Survey of Canada* (1969), pp. 69–39. DOI: 10.4095/106437. URL: https://doi.org/10.4095/106437.

[19] T. Bosak, A. H. Knoll, and A. P. Petroff. "The meaning of stromatolites". In: *Annual Review of Earth and Planetary Sciences* 41 (2013). ISSN: 00846597. DOI: 10.1146/annurev-earth-042711-105327.

[20] J. P. Grotzinger and D. H. Rothman. "An abiotic model for stromatolite morphogenesis". In: *Nature* 383.6599 (1996). ISSN: 00280836. DOI: 10.1038/383423a0.

[21] A. P. Petroff et al. "Biofilm Growth and Fossil Form". In: *Physical Review X* 3.4 (Nov. 2013), p. 041012. ISSN: 2160-3308. DOI: 10.1103/PhysRevX.3.041012.

[22] G. W. Ojakangas, S. M. Awramik, and M. C. Storrie-Lombardi. "Stromatolite photomorphogenesis: lighting up their shape". In: *International Journal of Astrobiology* 22.1 (Feb. 2023), pp. 33–56. ISSN: 1473-5504. DOI: 10.1017/S1473550422000313.

[23] J. Johnson and J. P. Grotzinger. "Affect of Sedimentation on Stromatolite Reef Growth and Morphology, Ediacaran Omkyk Member (Nama Group), Namibia". In: *South African Journal of Geology* 109.1-2 (June 2006), pp. 87–96. ISSN: 1012-0750. DOI: 10.2113/gssajg.109.1-2.87.

[24] A. Curtis et al. "Modelling Ediacaran metazoan–microbial reef growth". In: *Sedimentology* 68.5 (Aug. 2021), pp. 1877–1892. ISSN: 0037-0746. DOI: 10.1111/sed.12832.

[25] P. Szymczak et al. "Shapes of ideal stalagmites". In: *Proceedings of the National Academy of Sciences of the United States of America* 122.42 (2025). ISSN: 10916490. DOI: 10.1073/pnas.2513263122.

[26] B. Chopard, H. J. Herrmann, and T. Vicsek. "Structure and growth mechanism of mineral dendrites". In: *Nature* 353.6343 (1991). ISSN: 00280836. DOI: 10.1038/353409a0.

[27] Z. Hou et al. "Mineral dendrites: Indicators for geological aqueous environments". In: *Earth-Science Reviews* 270 (2025). ISSN: 00128252. DOI: 10.1016/j.earscirev.2025.105231.

[28] Z. Hou et al. "Three-dimensional mineral dendrites reveal a nonclassical crystallization pathway". In: *Geology* 51.7 (2023). ISSN: 19432682. DOI: 10.1130/G51127.1.

[29] G. Datseris, A. R. Vahdati, and T. C. DuBois. "Agents.jl: a performant and feature-full agent-based modeling software of minimal code complexity". In: *SIMULATION* 100.10 (Oct. 2024), pp. 1019–1031. ISSN: 0037-5497. DOI: 10.1177/00375497211068820.

[30] K. Hickman-Lewis et al. "Advanced two- and three-dimensional insights into Earth's oldest stromatolites (ca. 3.5 Ga): Prospects for the search for life on Mars". In: *Geology* 51.1 (Jan. 2023), pp. 33–38. ISSN: 0091-7613. DOI: 10.1130/G50390.1.

[31] T. A. Witten and L. M. Sander. "Diffusion-limited aggregation, a kinetic critical phenomenon". In: *Physical Review Letters* 47.19 (1981). ISSN: 00319007. DOI: 10.1103/PhysRevLett.47.1400.

[32] V. A. Petryshyn et al. "Stromatolite lamination frequency, Walker Lake, Nevada: implications for stromatolites as biosignatures". In: *Geology* 40.6 (2012), pp. 499–502. DOI: 10.1130/G32675.1.

[33] J. Szulc and B. Smyk. "Bacterially controlled calcification of freshwater Schizothrix-stromatolites: an example from the Pieniny Mts, Southern Poland". In: *Phanerozoic Stromatolites II*. Springer, 1994, pp. 31–51. DOI: 10.1007/978-94-011-1124-9_2.

[34] S. McMahon and J. Cosmidis. "False biosignatures on Mars: anticipating ambiguity". In: *Journal of the Geological Society* 179.2 (2022). ISSN: 00167649. DOI: 10.1144/jgs2021-050.

[35] N. McLoughlin, L. A. Wilson, and M. D. Brasier. "Growth of synthetic stromatolites and wrinkle structures in the absence of microbes – implications for the early fossil record". In: *Geobiology* 6.2 (Mar. 2008), pp. 95–105. ISSN: 1472-4677. DOI: 10.1111/j.1472-4669.2007.00141.x.

[36] J. Gong et al. "Morphogenesis of digitate structures in hot spring silica sinters of the El Tatio geothermal field, Chile". In: *Geobiology* 20.1 (2022). ISSN: 14724669. DOI: 10.1111/gbi.12471.